



OPEN ACCESS

EDITED BY

Songye Zhu,
Hong Kong Polytechnic University, Hong
Kong SAR, China

REVIEWED BY

Rodolfo Labernarda,
University of Calabria, Italy
Ruisheng Ma,
Beijing University of Technology, China

*CORRESPONDENCE

Mahdi Abdeddaim,
✉ m.abdeddaim@univ-biskra.dz

RECEIVED 16 May 2025

ACCEPTED 23 June 2025

PUBLISHED 09 July 2025

CITATION

Ghanemi NE, Abdeddaim M, Ounis A and
Basili M (2025) Neural network based active
control of base isolated structure considering
isolator nonlinearity.
Front. Built Environ. 11:1630131.
doi: 10.3389/fbuil.2025.1630131

COPYRIGHT

© 2025 Ghanemi, Abdeddaim, Ounis and
Basili. This is an open-access article
distributed under the terms of the [Creative
Commons Attribution License \(CC BY\)](#). The
use, distribution or reproduction in other
forums is permitted, provided the original
author(s) and the copyright owner(s) are
credited and that the original publication in
this journal is cited, in accordance with
accepted academic practice. No use,
distribution or reproduction is permitted
which does not comply with these terms.

Neural network based active control of base isolated structure considering isolator nonlinearity

Nour Elhouda Ghanemi¹, Mahdi Abdeddaim^{1*},
Abdelhafid Ounis¹ and Michela Basili²

¹LARGHYDE Laboratory, Department of Civil Engineering and Hydraulics, Faculty of Architecture, Urbanism, Civil Engineering and Hydraulics, Biskra University, Biskra, Algeria, ²Department of Engineering and Sciences, Universitas Mercatorum, Rome, Italy

Introduction: Hybrid control systems combining passive and active strategies have emerged as effective solutions to enhance structural resilience during earthquakes. Recent advancements in smart structures integrate active tuned mass dampers (ATMDs) for precise dynamic response control and seismic hazard mitigation. Simultaneously, artificial intelligence (AI), particularly machine learning algorithms, has opened new frontiers in structural control.

Methods: This study proposes a novel AI-based approach for structures equipped with nonlinear base isolation and an ATMD. An artificial neural network (ANN) is employed, trained via supervised learning using the Levenberg-Marquardt backpropagation algorithm to minimize displacement demands during strong earthquakes. The ANN-driven controller aims to achieve significant response reduction with fewer sensors than traditional algorithms while enhancing robustness against signal time delays and white noise contamination. For validation, an ATMD is installed at the base isolation layer of an 8-story benchmark building. The ANN controller's performance is evaluated under near-field and far-field seismic excitations and compared with a conventional linear quadratic regulator (LQR)-controlled ATMD and a classical tuned mass damper (TMD). Robustness tests include time delays and white noise in input signals.

Results: The results demonstrate that the ANN-driven ATMD controller notably reduces key dynamic response parameters, including peak base acceleration, displacement, velocity, inter-story drift, maximum drift, and base shear, under both near-field and far-field earthquake scenarios. Furthermore, the ANN controller maintains high performance even when subjected to signal time delays and white noise contamination, underscoring its robustness. Importantly, these improvements are attained while utilizing fewer sensors than the LQR controller, highlighting the practicality and cost-effectiveness of the proposed method.

Discussion: The proposed ANN controller achieves performance comparable to the full-state LQR controller but requires fewer sensors, enhancing practicality and cost-effectiveness for real-world applications. This approach demonstrates

superior robustness against signal imperfections while maintaining high seismic response mitigation efficacy.

KEYWORDS

hybrid control, artificial intelligence, active tuned mass damper, base isolator, artificial neural network, linear quadratic regulator, signal time delay, white noise

1 Introduction

In the field of civil engineering, mitigating structural damage caused by seismic and wind actions is of critical importance. Earthquakes, in particular, pose significant threats to the stability of buildings and infrastructure, making the development and implementation of advanced control systems essential for enhancing structural resilience (El Ouni et al., 2022; Elias et al., 2025).

Control systems are generally classified into four categories: passive, active, semi-active, and hybrid (Fisco and Adeli, 2011a; Fisco and Adeli, 2011b). Passive control systems play a key role in seismic protection, particularly in the area of base isolation. These systems, such as base isolation (BI), tuned mass dampers (TMDs), and energy dissipation devices, operate without the need for external energy sources (Djerouni et al., 2020; Elia et al., 2017; Mazza et al., 2024; Mazza et al., 2023).

Base Isolation Systems (BIS) function by decoupling the superstructure's dynamic response from that of the ground. This is achieved through the introduction of a laterally flexible isolation layer between the foundation and the superstructure. The effectiveness of BIS has been extensively investigated in the literature (Sapountzakis et al., 2024; Skinner et al., 1993; Naeim and Kelly, 1999; Charrouf et al., 2024; Mazza and Labernarda, 2022). Despite their proven reliability and simplicity, these techniques are inherently limited by their passive nature, which prevents them from adapting to seismic events not considered during the design stage. To overcome these limitations, hybrid control systems, which can combine passive and active/semi-active control mechanisms, have been proposed as a more adaptable and effective solution in certain scenarios (Djedoui et al., 2017; Banerjee and Matsagar, 2023; Cheng and Jiang, 1998; Zahedin Labaf et al., 2023). Given the often nonlinear behavior of many passive devices, hybrid systems are particularly valuable for actively managing nonlinearities and inelastic hysteretic responses (Yang et al., 1992; Li et al., 2021). The integration of active control elements into base-isolated systems can help mitigate some of the drawbacks associated with nonlinear BIS, especially the large displacements that may occur under severe earthquake excitations (Heertjes and van de Wouw, 2006; Lee and Kawashima, 2007; Subasri et al., 2013; Gu et al., 2017).

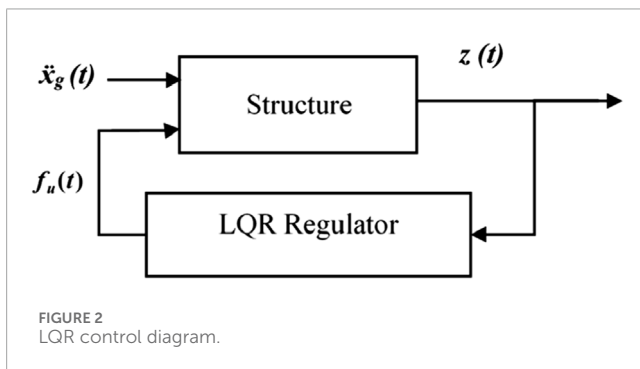
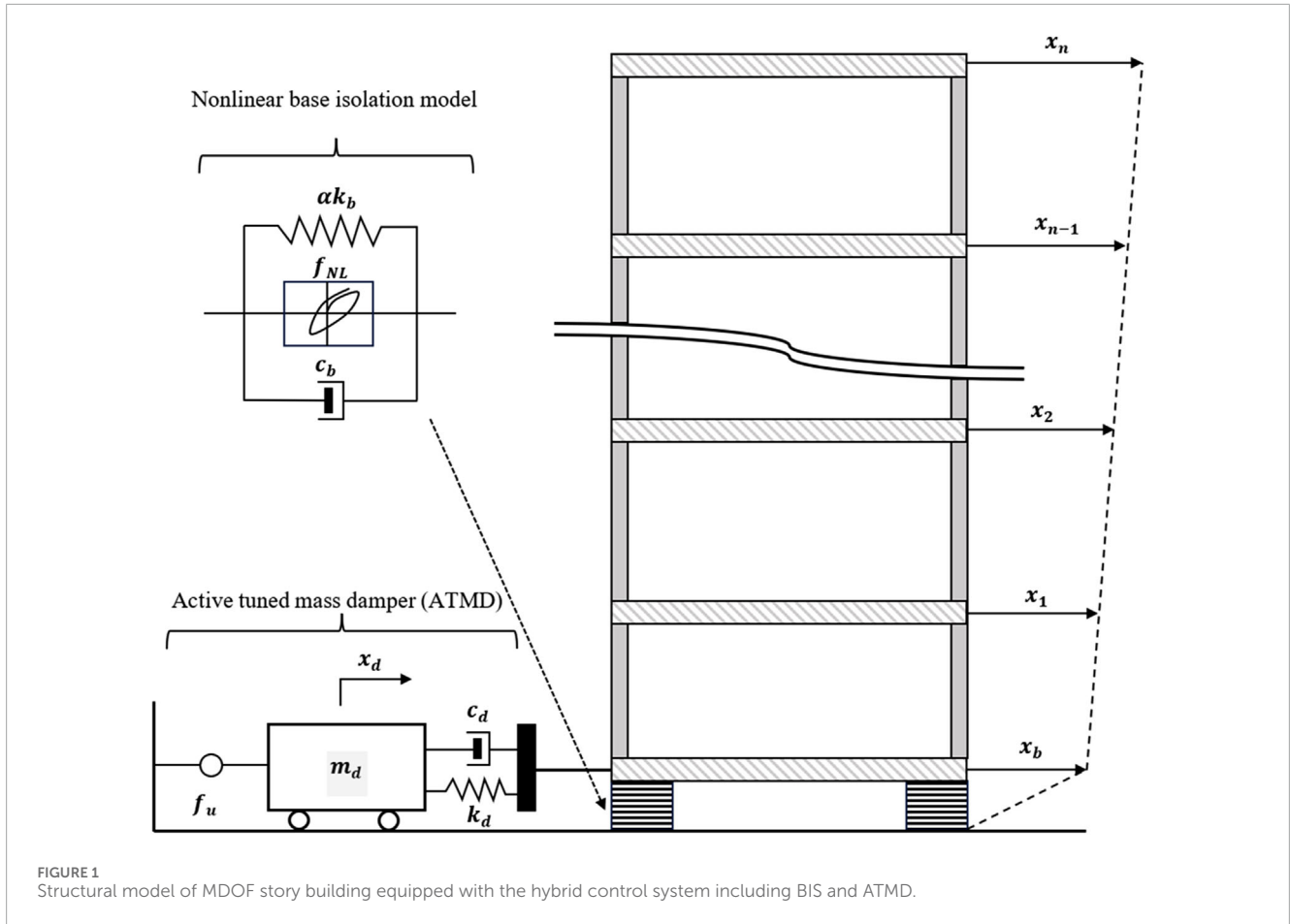
Active control systems utilize sensors, actuators, and sophisticated control algorithms to dynamically respond to seismic forces, adjusting the structural response in real-time. One of the most used devices is the active tuned mass damper (ATMD), which has emerged as a viable solution for reducing unwanted vibrations in multistory buildings during seismic events (Sabetahd et al., 2022; Chang and Soong, 1980; Ümütlü et al., 2021). Researchers such as Li et al. (Linderman and Spencer, 2016) have demonstrated the effectiveness of ATMDs in high-rise buildings, while Linderman and Spencer have explored their integration with wireless sensor networks in civil structures (Linderman and Spencer, 2016). Control

requirements for ATMD systems can be substantial. To address this challenge, various algorithms have been developed to optimize the control effort and enhance overall system performance. Among the most widely used are proportional-integral-derivative (PID) controllers (Djedoui et al., 2016; Ulusoy et al., 2021) and the linear quadratic regulator (LQR), first introduced in the 1960s (Kalman, 1960). This method has since been widely applied in active and semi-active control systems (Amezquita-Sanchez et al., 2014; Elias et al., 2023; Hashemi et al., 2022). The main goal of the LQR approach is to determine an optimal control law that minimizes a predefined quadratic cost function, which typically balances the system's performance and the energy required for control. By systematically weighing the relative importance of state deviations and control efforts, the LQR provides a feedback gain matrix that ensures efficient performance with constrained energy input, making it especially suitable for real-time structural control applications. LQR is pivotal in controlling multiple-input multiple-output (MIMO) systems (Islam et al., 2003; Phillips and Sahin, 2014; Pandey and Laxmi, 2015). However, its practical application is challenged by the considerable sensor requirements, often limited by real-world constraints on sensor availability (Ghanemi et al., 2024).

Integrating hybrid control for a multi-degree-of-freedom (MDOF) structure equipped with BIS offers a promising solution for reducing excessive seismic displacement at the base isolation level (Shin et al., 2020). However, in this context, a significant challenge is the necessity for nonlinear adaptive control strategies to account for the hysteresis or friction mechanism typically introduced by the base-isolation system. Classical control methods, such as PID and LQR controllers, have shown limitations in effectively managing time-varying and nonlinear systems. To address these challenges, a novel approach involving artificial intelligence (AI) control methods is proposed.

In recent decades, researchers have made significant strides in AI, which has greatly enhanced the performance of structural systems in areas such as monitoring, controlling, evaluating, and response mitigation. Lu et al. (2012) performed a survey examining various AI techniques, such as evolutionary computation, fuzzy logic, neural networks, and swarm intelligence. Aldwaik and Adeli (2014) presented a multiparadigm learning approach, showing that integrating neural networks, genetic algorithms, fuzzy sets, and parallel processing can significantly boost performance. Mardani et al. (2015) reviewed the uses and approaches of fuzzy multi-criteria decision-making methods, while Zhang and Xue (2023) examined the latest developments in optimizing high-rise buildings. Moreover, studies have explored the application of random forests for safeguarding structures from external disturbances (Smarra et al., 2020; Di Girolamo et al., 2020).

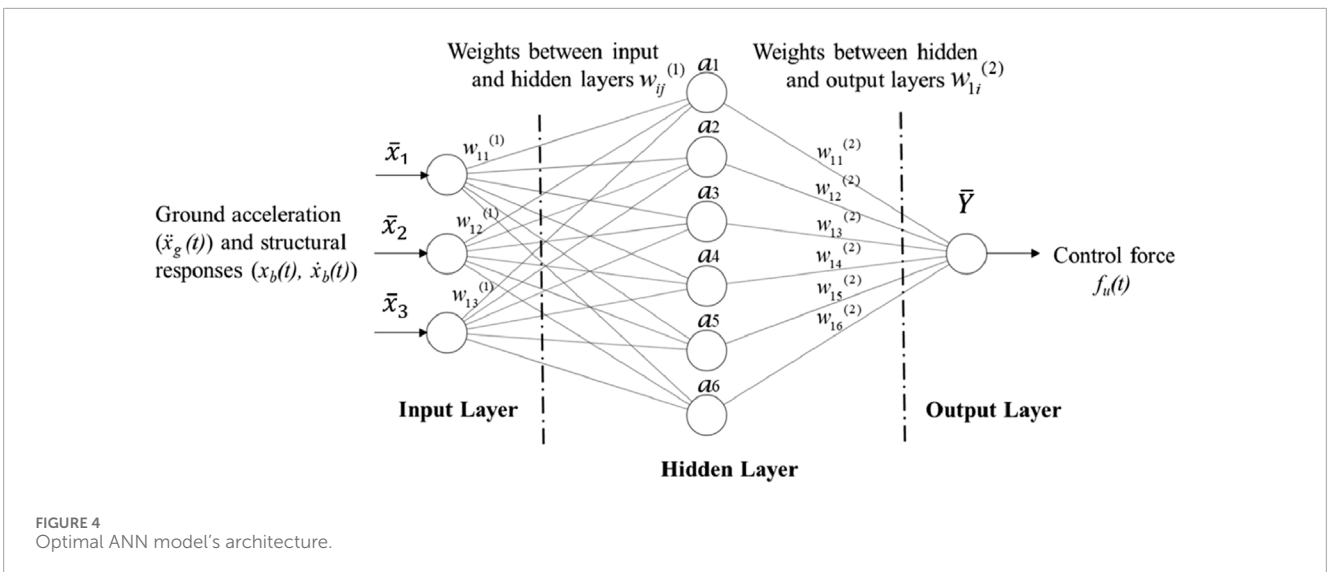
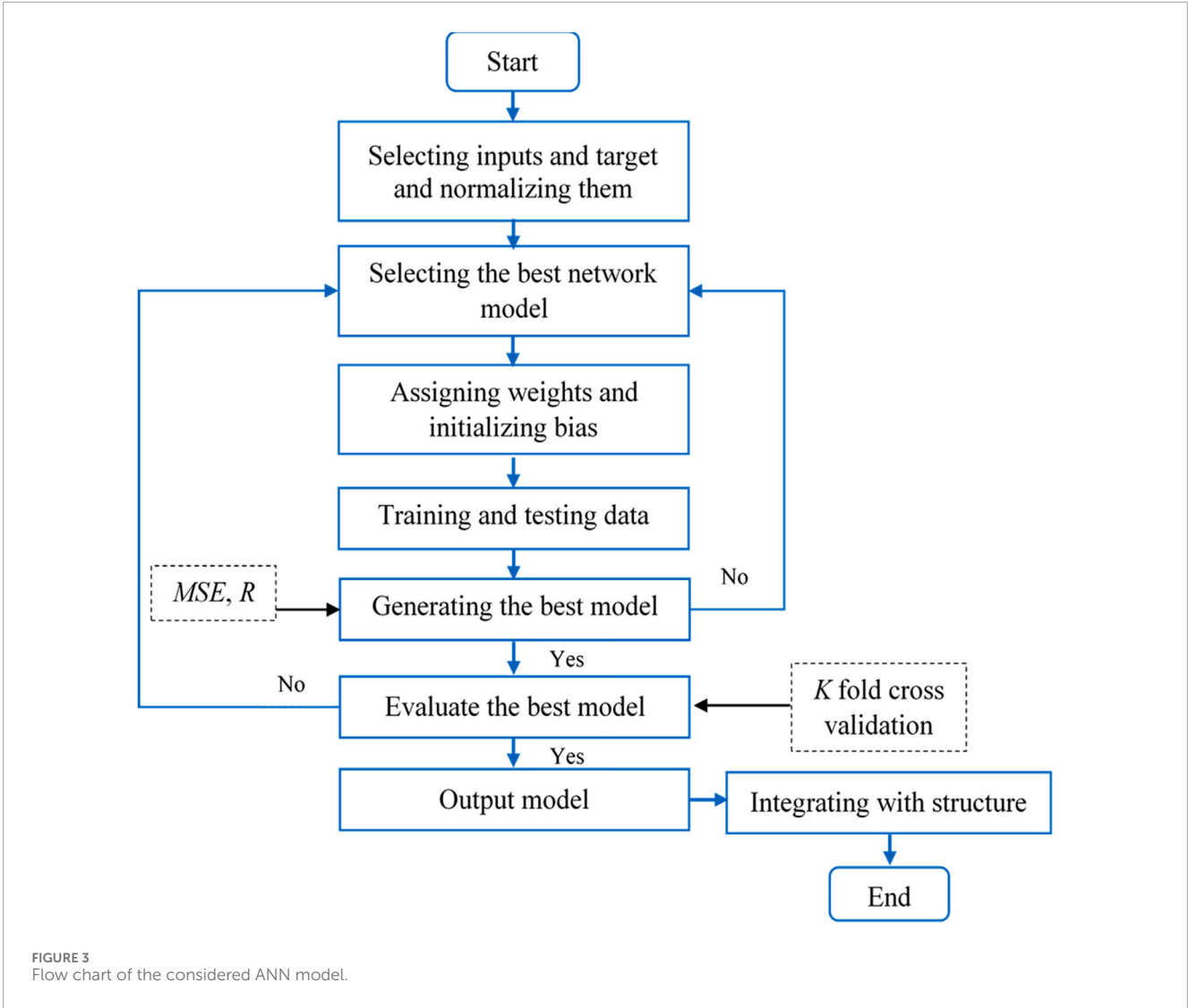
One of the most widely used AI techniques is Artificial Neural Networks (ANN). The utilization of ANN models in managing seismic responses has led to notable progress, particularly in



mitigating structural oscillations (Jhang et al., 2018; Yang et al., 2006). A fundamental aspect of ANN controllers is their precision in approximating nonlinear functions, rendering them well-suited for intricate systems like multistory buildings (Conte et al., 1994; Blachowski and Pnevmatikos, 2018). For instance, ANNs have been used to develop intelligent systems that adapt in real-time (Jamil et al., 2021), Chang and Sung evaluated enhanced vibration mitigation in a nonlinear building using a neuro-controller (Chang and Sung, 2019), and Liut et al. (1999) developed a neural network controller, trained through a force-matching technique, to operate a tuned-mass damper confirming its functionality. The use of ANN in assessing bridge risks has been thoroughly investigated (Ying et al.,

2009; Neves et al., 2017). Additionally, ANN has been employed to mitigate structural responses to seismic risks (Ghanemi et al., 2024; Ghanemi et al., 2023; Blachowski and Pnevmatikos, 2018; Radmard Rahmani et al., 2019; Brancati et al., 2020). Furthermore, Sanad and Saka (2001) applied ANNs to predict the maximum shear strength of reinforced concrete beams. The time delay method is widely used for training ANNs (Chen and Chien, 2020), yet its specific effects on structural responses remain largely unexplored. This gap highlights the need for research that examines how these methods influence the overall performance of the system's response.

The primary focus of this study is the development of an AI-based controller aimed at enhancing the functionality of nonlinear base-isolated structures while simultaneously reducing sensor requirements and improving robustness against external disturbances. Specifically, the proposed approach integrates an ANN controller with an ATMD to mitigate the seismic response of a base-isolated structure. The ANN controller is trained using data generated by an LQR based on one earthquake signal, enabling it to replicate near-optimal control strategies while significantly reducing the need for full-state observation. Unlike conventional LQR controllers, which typically require a large number of sensors to monitor all state variables, the ANN controller operates effectively using fewer sensors, directly addressing concerns about ATMD implementation complexity and cost by minimizing hardware requirements. In addition to performance under ideal conditions, the proposed ANN-driven ATMD system is also evaluated under



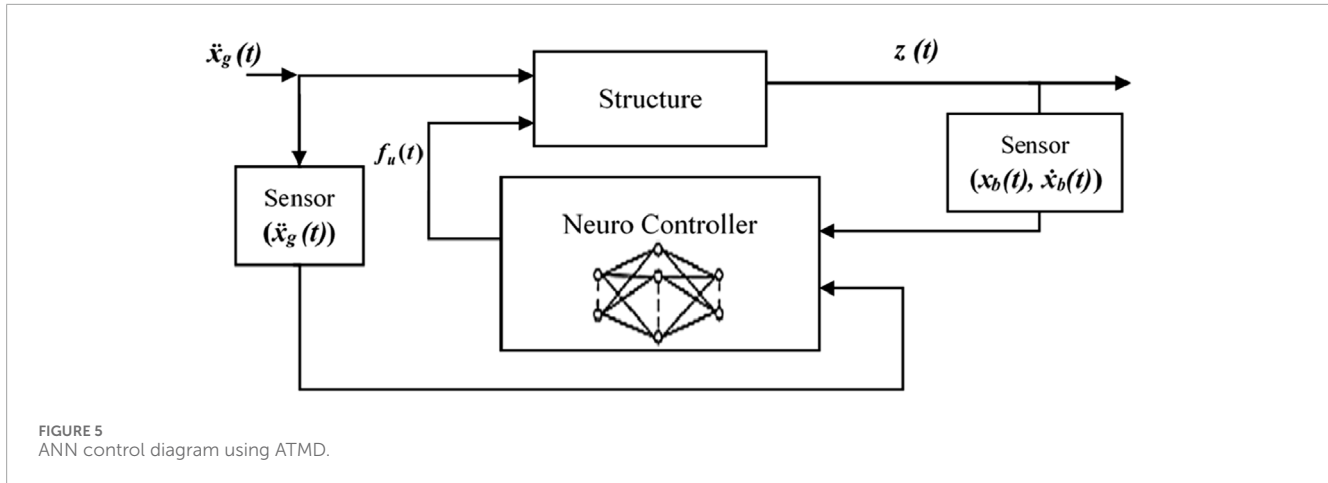


FIGURE 5 ANN control diagram using ATMD.

TABLE 1 Dynamic parameters of the structure.

Floor	Mass (tons)	Stiffness (kN/m)	Damping (kNs/m)
1	345.6	3.40×10^5	490
2	345.6	3.26×10^5	467
3	345.6	2.85×10^5	410
4	345.6	2.69×10^5	386
5	345.6	2.43×10^5	348
6	345.6	2.07×10^5	298
7	345.6	1.69×10^5	243
8	345.6	1.37×10^5	196

TABLE 2 BIS parameters.

Properties	Value	Unit
m_b	450	tons
c_b	26.17	kNs/m
k_b	18,050	kN/m
α_b	60	%
D_{yb}	4	cm
A_b	1	—
β_b	0.5	—
n_b	3	—
γ_b	0.5	—

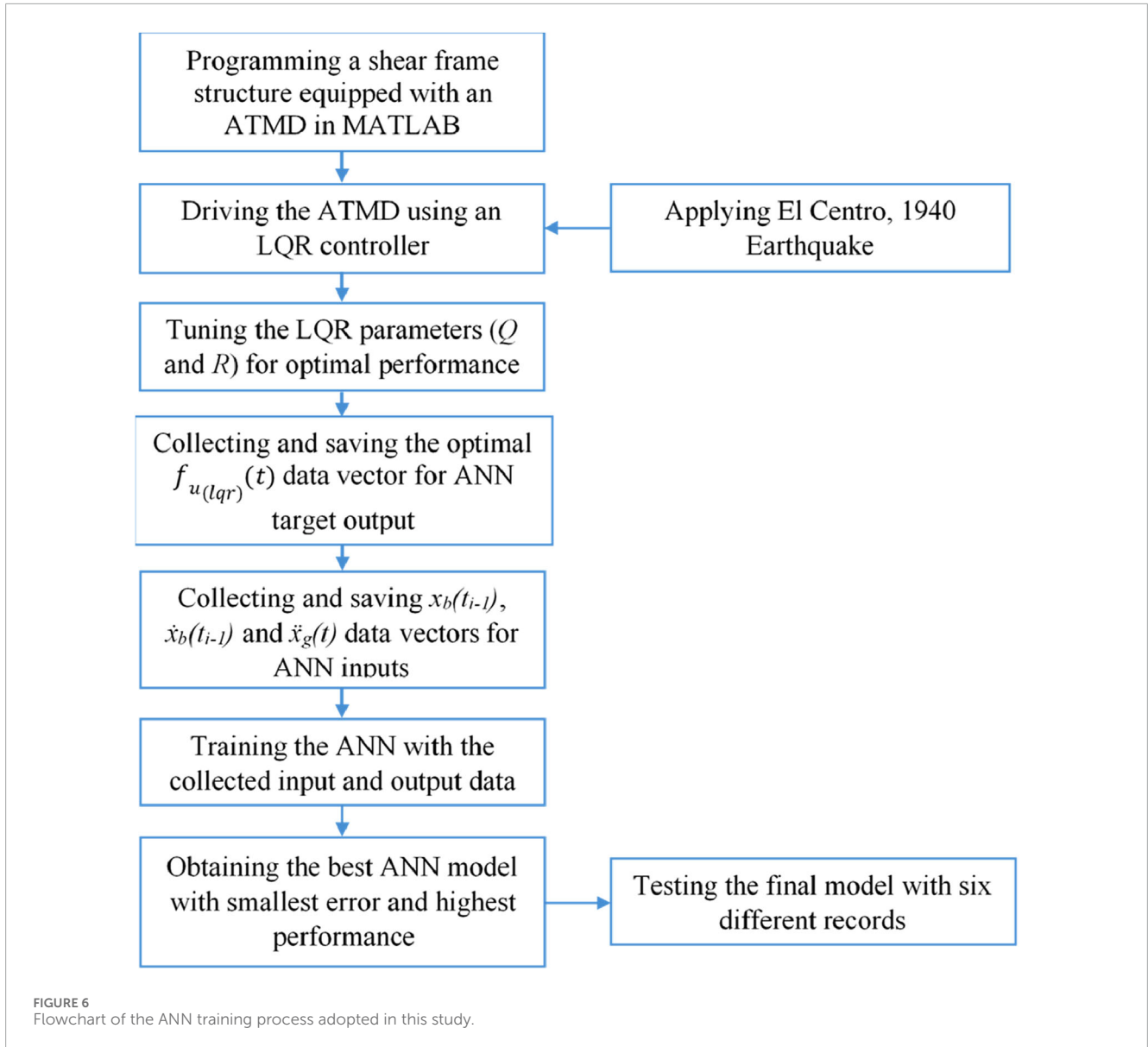
signal time delays and white noise contamination to proactively resolve feasibility challenges and verify its robustness in realistic operating environments. This dual focus on sensor reduction and delay/noise tolerance ensures practical viability without compromising control efficacy. The methodology is applied to an 8-story nonlinear base-isolated benchmark building subjected to both near-field and far-field earthquake records. The performance of the ANN-based controller is systematically compared with that of a classical TMD and a conventional LQR-controlled ATMD. Furthermore, to validate the generalizability of the proposed approach, the ANN controller is tested under six additional earthquake records beyond the one adopted in the training phase. By demonstrating consistent performance across diverse seismic events while mitigating implementation barriers, this work establishes a balanced framework for intelligent vibration control systems.

The remainder of the paper is organized as follows. Section 2 presents the mathematical modeling of the system, describing both the LQR controller and the ANN training process. Section 3 details the numerical study, including the description of the benchmark building model, the tuning of the ATMD, the properties of the base-isolated system, the tuning processes for both the LQR and ANN controllers, and the earthquake dataset used for validation. Section 4 discusses the results, highlighting the effectiveness of the proposed controller and analyzing the impact of time delay and noise on the system’s performance. Finally, Section 5 concludes the paper, summarizing the main findings and suggesting directions for future research.

2 Mathematical model

Let’s consider an n-DOF structure equipped with a nonlinear BIS combined with an ATMD (Figure 1) exposed to earthquake ground acceleration. The BIS is modeled as a rigid mass m_b , with horizontal displacement x_b and base isolators. The restoring force $F_b(t)$ exerted by the isolators accounts for both linear and nonlinear behavior modeled as reported in Yang et al. (1994) as it can be seen in Equation 1:

$$F_b(t) = c_b \dot{x}_b(t) + \alpha_b k_b x_b(t) + (1 - \alpha_b) k_b D_{yb} v_b(t) \tag{1}$$



where c_b and k_b respectively represent the BIS viscous damping coefficient and elastic stiffness, α_b is the ratio between the post-yielding to pre-yielding stiffness, D_{yb} signifies the yield deformation and v_b symbolizes the non-dimensional variable describing the hysteretic component of the deformation according to Bouc-Wen law (Wen, 1976; Wen, 1989; Ismail et al., 2009) the first derivative of v_b is shown in Equation 2 as follow:

$$\dot{v}_b = D_{yb}^{-1} [A_b \dot{x}_b - \beta_b |\dot{x}_b| |v_b|^{\eta_b - 1} v_b - \gamma_b \dot{x}_b |v_b|^{\eta_b}] \quad (2)$$

where the overdot denotes the derivative with respect to time. The parameter η_b influences the smoothness of the force-deformation curve, while the parameters $A_b, \beta_b,$ and γ_b control both the scale and the shape of the hysteresis loop.

It is possible to decompose the restoring force $F_b(t)$ (Equation 3) into two distinct components, characterized by a linear segment $f_L(t)$ (Equation 4) and a nonlinear segment $f_{NL}(t)$ (Equation 5):

$$F_b(t) = f_L(t) + f_{NL}(t) \quad (3)$$

$$f_L(t) = c_b \dot{x}_b(t) + \alpha_b k_b x_b(t) \quad (4)$$

$$f_{NL}(t) = (1 - \alpha_b) k_b D_{yb} v_b(t) \quad (5)$$

In order to minimize the BIS displacement, an ATMD with mass m_d and horizontal displacement x_d is attached to it. The ATMD mass is connected at one side to the BIS through an elastic stiffness k_d and a viscous damping coefficient c_d , and at the other side to the actuator, which exerts its active control force f_u . The active control force impacts the structure by directly influencing its own response, which, in turn, modifies the BIS motion to enhance overall stability. By managing the isolator's motion, it can effectively control the response of the entire superstructure.

Equation 6 shows the equation of motion that governs the resultant $(n + 2)$ -DOF system is expressed as:

$$M\ddot{\mathbf{x}}_t + L\dot{\mathbf{x}}_t + K\mathbf{x}_t + f_{NL}(t)\mathbf{H} = -M\mathbf{r}\ddot{x}_g + \mathbf{d}f_u \quad (6)$$

TABLE 3 FEMA unscaled ground motion records.

RSN	Name	Year	Mag	Component	PGA (g)	PGV (cm/s)
Far Fault						
1244	Chi-Chi	1999	7.6	CHICHI/CHY101-E	0.44	115
68	San Fernando	1971	6.6	SFERN/PEL090	0.21	19
No Pulse Near-Fault						
1176	Kocaeli	1999	7.5	KOCAELI/YPT_180	0.31	73
2114	Denali	2002	7.9	DENALI/ps10_289	0.33	126.4
Pulse Near-Fault						
879	Landers	1992	7.3	LANDERS/LCN_239	0.79	140.3
1165	Kocaeli	1999	7.5	KOCAELI/IZT_270	0.22	29.8

$\mathbf{x}_t = \{x_b \ x_1 \ x_2 \ \dots \ x_n \ x_d\}^T$ represents the displacement vector, whereas \mathbf{M} , \mathbf{L} , and \mathbf{K} respectively represent the system mass, damping, and stiffness matrix as it can be seen in Equations 7–9. \mathbf{r} is the influence vector that captures the effect of ground acceleration \ddot{x}_g . The vector \mathbf{d} (Equation 10) specifies the location where the control force f_u is applied, note that a null \mathbf{d} will result in the mathematical formulation of a classical TMD. Meanwhile, \mathbf{H} (Equation 10) represents the distribution of the base isolation force on the structure.

Matrices \mathbf{M} , \mathbf{L} , and \mathbf{K} have the following expressions:

$$\mathbf{M} = \begin{bmatrix} m_b & 0 & 0 & 0 & 0 & 0 & 0 \\ 0 & m_1 & 0 & 0 & 0 & 0 & 0 \\ 0 & 0 & m_2 & 0 & 0 & 0 & 0 \\ 0 & 0 & 0 & \ddots & 0 & 0 & 0 \\ 0 & 0 & 0 & 0 & m_{n-1} & 0 & 0 \\ 0 & 0 & 0 & 0 & 0 & m_n & 0 \\ 0 & 0 & 0 & 0 & 0 & 0 & m_d \end{bmatrix} \quad (7)$$

$$\mathbf{L} = \begin{bmatrix} c_b + c_1 + c_d & -c_1 & 0 & 0 & 0 & 0 & -c_d \\ -c_1 & c_1 + c_2 & -c_2 & 0 & 0 & 0 & 0 \\ 0 & -c_2 & c_2 + c_3 & -c_3 & 0 & 0 & 0 \\ 0 & 0 & -c_3 & \ddots & \ddots & 0 & 0 \\ 0 & 0 & 0 & \ddots & c_{n-1} + c_n & -c_n & 0 \\ 0 & 0 & 0 & 0 & -c_n & c_n & 0 \\ -c_d & 0 & 0 & 0 & 0 & 0 & c_d \end{bmatrix} \quad (8)$$

$$\mathbf{K} = \begin{bmatrix} \alpha_b k_b + k_1 + k_d & -k_1 & 0 & 0 & 0 & 0 & -k_d \\ -k_1 & k_1 + k_2 & -k_2 & 0 & 0 & 0 & 0 \\ 0 & -k_2 & k_2 + k_3 & -k_3 & 0 & 0 & 0 \\ 0 & 0 & -k_3 & \ddots & \ddots & 0 & 0 \\ 0 & 0 & 0 & \ddots & k_{n-1} + k_n & -k_n & 0 \\ 0 & 0 & 0 & 0 & -k_n & k_n & 0 \\ -k_d & 0 & 0 & 0 & 0 & 0 & k_d \end{bmatrix} \quad (9)$$

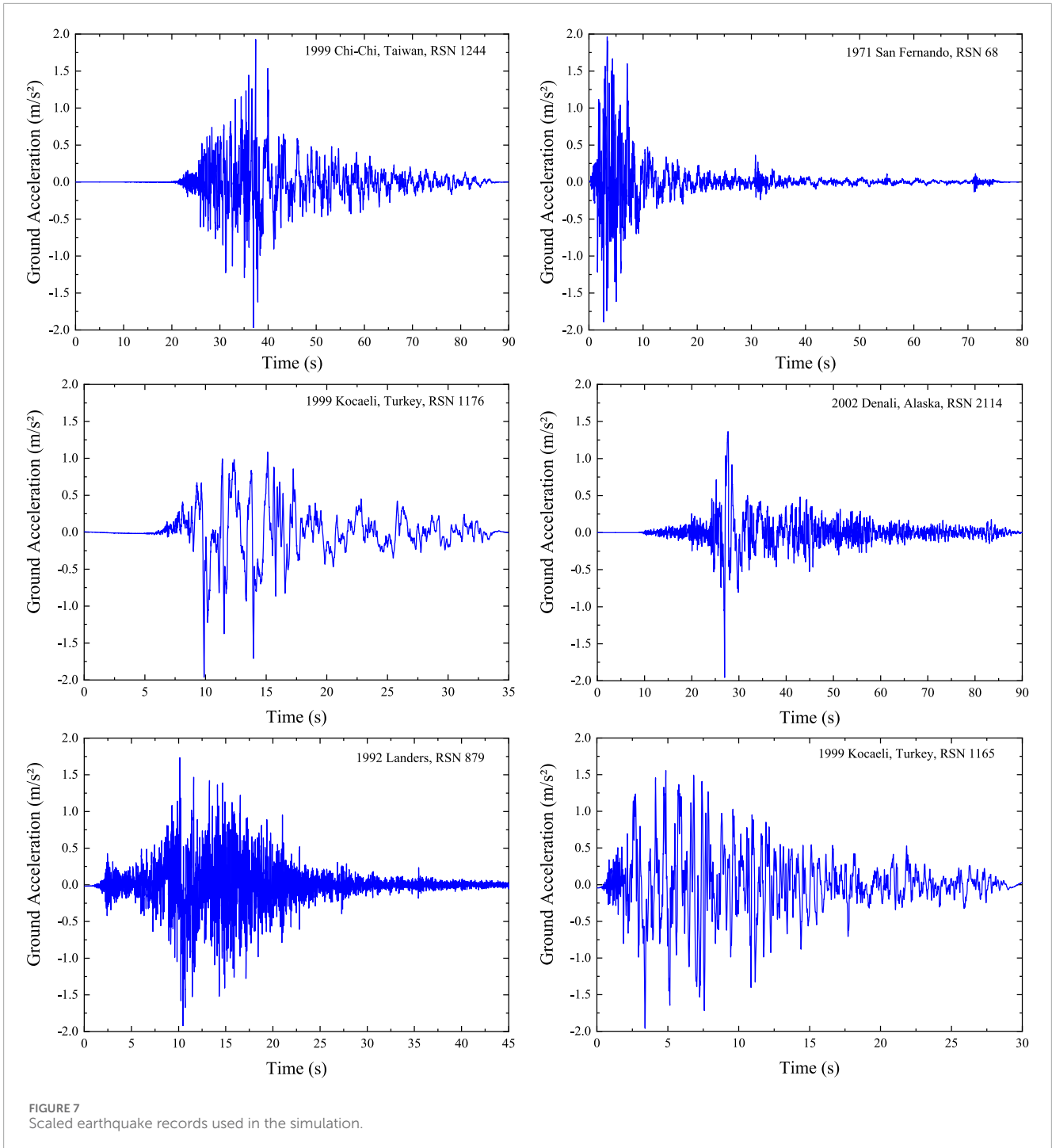
vectors \mathbf{d} and \mathbf{H} , of $((n+2) \times 1)$ dimensions, assume the form:

$$\mathbf{d} = \begin{bmatrix} 0 \\ 0 \\ \vdots \\ 0 \\ 0 \\ 0 \\ 1 \end{bmatrix}, \mathbf{H} = \begin{bmatrix} 1 \\ 0 \\ \vdots \\ 0 \\ 0 \\ -1 \end{bmatrix} \quad (10)$$

Let's note that the linear component of the BIS restoring force $f_{l1}(t)$ is collected in the matrices \mathbf{L} and \mathbf{K} . The second-order nonlinear (Equation 6) can be transformed into a first-order nonlinear equation (Equation 11), known as the state-space representation in the following manner:

$$\begin{cases} \dot{\mathbf{z}}(t) = \mathbf{A}\mathbf{z}(t) + \mathbf{B}\mathbf{u}(t) \\ \mathbf{y}(t) = \mathbf{C}\mathbf{z}(t) + \mathbf{D}\mathbf{u}(t) \end{cases} \quad (11)$$

$\mathbf{z}(t) = [\dot{\mathbf{x}}_t(t) \ \mathbf{x}_t(t)]^T$ represents the full state of the system, encompassing velocity and displacement vectors, $\mathbf{u}(t) = [f_u(t) \ \ddot{x}_g(t)]^T$ is the input vector collecting the ATMD force and



the seismic acceleration, $y(t)$ is the output vector. Matrices A and B correspond to the state and the input matrix (Equations 12, 13), respectively defined as:

$$A = \begin{bmatrix} -M^{-1}L & -M^{-1}K \\ E & 0 \end{bmatrix} \tag{12}$$

$$B = \begin{bmatrix} -M^{-1}d & E \\ 0 & 0 \end{bmatrix} \tag{13}$$

C and D are the output matrix and the feedthrough matrix, respectively, and can vary depending on the choice of the output vector.

2.1 The trainer controller LQR

LQR controller is one of the most widely used classical control algorithms for active control (Moghaddasie and Jalaeefar, 2019).

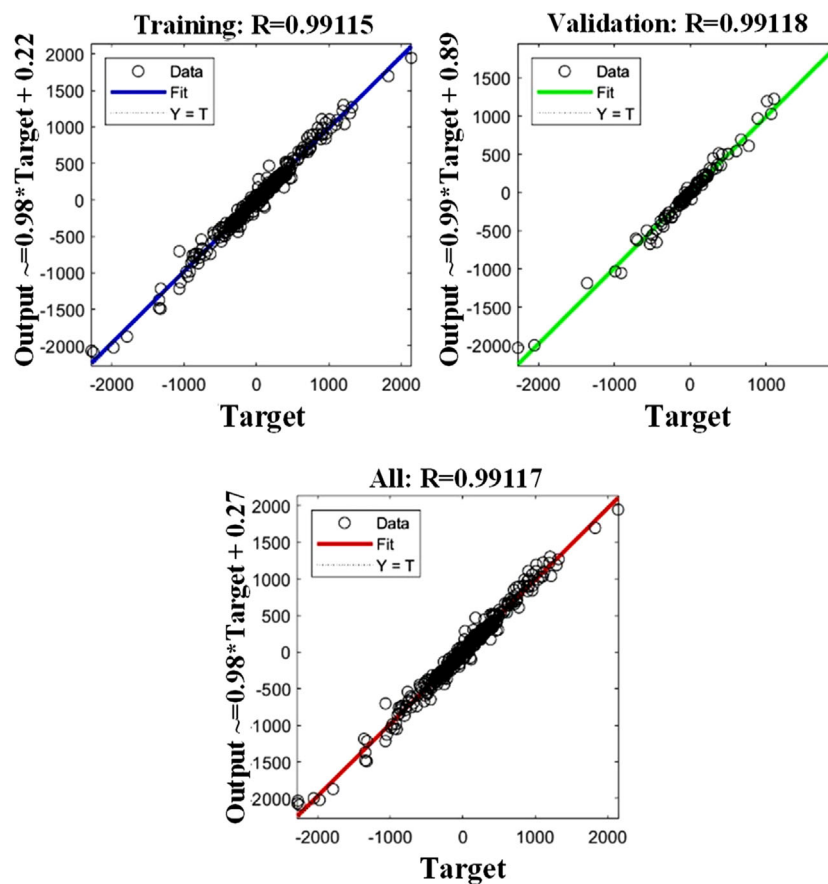


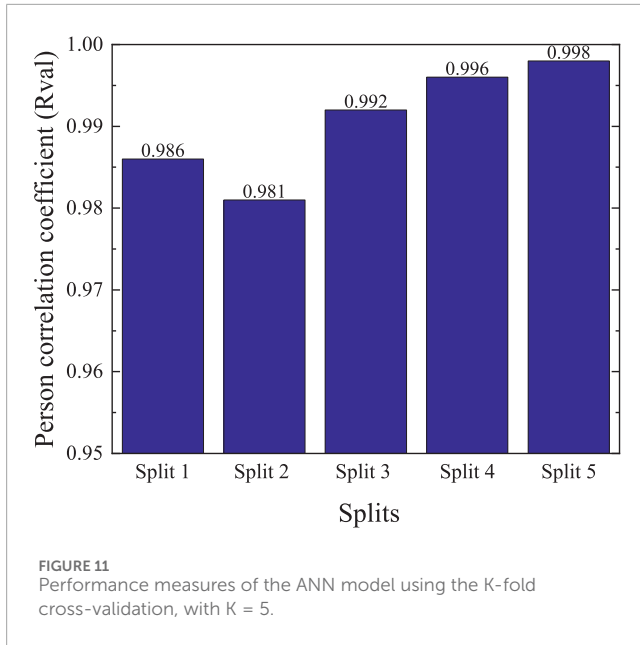
FIGURE 10
Scatter plots between predicted and measured f_u in the optimal ANN model (3 6 1).

3. Model Initialization: initialize the ANN model with randomly assigned weights and biases.
4. Forward Propagation - Hidden Layer: compute the activations of the hidden layer by applying an activation function to the weighted sum of inputs plus biases.
5. Forward Propagation - Output Layer: using the output of the hidden layer to compute the final output of the network, again applying weights, biases, and an appropriate activation function.
6. Training and optimization: adjust weights and biases through a learning algorithm, minimizing the loss function.
7. Model Evaluation: Assess model performance using suitable statistical metrics. If the model does not perform well, readjust the weights and biases and iterate; otherwise, finalize the weights and compute the final output.
8. Cross-Validation: perform K-fold cross-validation to verify the generalization capability of the model and check whether overfitting or underfitting occurs. If either is detected, the model is retrained.
9. Model Selection and Deployment: finalize the trained ANN model based on the best-performing configuration. Integrate the trained model into the control loop of the ATMD system for real-time prediction of the control force.

A flowchart detailing the major steps of the procedure can be seen in [Figure 3](#).

The current study employed a multilayer ANN architecture, visually represented in [Figure 4](#), structured with three layers: an input layer, a hidden layer, and an output layer.

The input data utilized in the input layer include the base displacement and its velocity, respectively $x_b(t)$ and $\dot{x}_b(t)$, and the ground motion acceleration $\ddot{x}_g(t)$ taken from an earthquake record characterized by a wide frequency range. Optimized over iterations, the hidden layer has six nodes, and the output layer has one node (\bar{Y}) representing the LQR control force $f_u(t)$ trained with target data of an optimal LQR control force. Therefore, the model is represented as [Fisco and Adeli \(2011a\)](#), [Fisco and Adeli \(2011b\)](#), [Djerouni et al. \(2020\)](#) and [Elia et al. \(2017\)](#). The layers in the neural network are interconnected by weights, which are adjusted during the training process to minimize the error between the ANN model's output and the desired target LQR control force. The connections between the input and hidden layers are represented by weight terms $w_{ij}^{(1)}$, where i corresponds to the index of the hidden neuron and j to the input neuron. Similarly, the connections between the hidden and output layers are defined by the weight terms $w_{li}^{(2)}$, where i denotes the hidden neuron index. The hidden layer consists of activation neurons a_i , which processes the weighted sum of the inputs through a nonlinear activation function $f(\bar{g}_i)$, enhancing the network's ability



to capture complex relationships in the data. This architecture allows the ANN to learn and replicate the control strategy of the LQR controller effectively.

For training and optimization, the network configuration implemented the backpropagation algorithm, a widely used technique for training neural networks, in conjunction with the TANSIG (hyperbolic tangent sigmoid) activation function (Sibi et al., 2013). These choices were pivotal in the model's ability to effectively learn and adapt to the complexities of the dataset under investigation. The equation of the activation (Equation 19) function is written as follows:

$$f(\bar{g}_i) = \frac{2}{(1 + e^{-2\bar{g}_i})} - 1 \quad (19)$$

The output of the first layer is obtained by applying the activation function (Equation 20):

$$a_i = f(\bar{g}_i) = f\left(\sum_{j=1}^3 w_{ij}^{(1)} \bar{x}_j + b_i^{(1)}\right) \quad (20)$$

Finally, the final output is determined as (Equation 21):

$$\bar{Y} = \sum_{i=1}^6 w_{1i}^{(2)} a_i + b^{(2)} \quad (21)$$

In this scenario, \bar{x}_j represents the input features, while $w^{(1)}$ and $w^{(2)}$ correspond to the weights associated with the first and hidden layers, respectively. Similarly, $b^{(1)}$ and $b^{(2)}$ denote the biases for the first and second layers.

To guarantee the robustness of the model during the training phase, the dataset was divided into training and validation subsets, with 80% dedicated to training the neural network. This allowed for effective pattern recognition. The remaining 20% was used for validation, providing an evaluation of the model's accuracy on new data. The Levenberg-Marquardt backpropagation technique (trainlm) (Reynaldi et al., 2012) from MATLAB's Neural Network Toolbox was selected for its proficiency in optimizing parameters and reducing training errors.

According to the model training process, the mean squared error (MSE) (Equation 22) and the correlation coefficient (R) (Equation 23) are utilized as performance metrics and evaluated as:

$$MSE = \frac{1}{N} \sum_{i=1}^N (Y_{tar,i} - Y_{out,i})^2 \quad (0 < MSE < \infty) \quad (22)$$

$$R = \frac{\sum_{i=1}^N ((Y_{tar,i} - \bar{Y}_{tar})(Y_{out,i} - \bar{Y}_{out}))}{\sqrt{\sum_{i=1}^N ((Y_{tar,i} - \bar{Y}_{tar})^2 (Y_{out,i} - \bar{Y}_{out})^2)}} \quad (-1 < R < 1) \quad (23)$$

where $Y_{tar,i}$, $Y_{out,i}$, \bar{Y}_{tar} , \bar{Y}_{out} correspond to the target, output, mean target, and mean output, respectively, whereas N represents the dataset size to measure the performance of the model and assess the error for each split. According to Smith (1986), the evaluation criteria for (R) include the following limit:

- $|R| < 0.2$ Weak correlation.
- $0.2 \leq |R| < 0.8$ Correlation exists.
- $|R| \geq 0.8$ Strong Correlation.

Following the selection of the optimal model with the optimal node's number according to statistical performance, the K-fold cross-validation approach (Kohavi, 1995) was employed to assess the model's capability prediction. K-fold cross-validation is a method used to evaluate a machine learning model's performance by dividing the dataset into k equally sized subsets. The model is trained k times, each time using $(k - 1)$ folds for training and the remaining fold for validation. This ensures that each fold serves as the validation set exactly once.

In this study, 5-fold cross-validation was adopted, as it offers a good compromise between computational efficiency, bias, and variance, making it a standard choice for model evaluation.

Figure 5 illustrates the active control feedback, in which the ANN controller actuates the ATMD to mitigate structural vibrations. The system comprises three primary sensors: one measuring the base layer displacement, another measuring the base layer velocity, and a third measuring the ground acceleration. The sensor data are fed into the ANN controller, which processes the inputs and determines the appropriate control force. This control force is applied to the structure to counteract the vibrations. The structure's response is continuously monitored and fed back into the neuro controller, creating a closed-loop system. The ANN controller dynamically adjusts the damping force based on real-time feedback, ensuring optimal vibration suppression and enhancing structural stability and performance under various dynamic conditions. The ANN controller dynamically adjusts the damping force in real-time based on feedback, ensuring effective vibration suppression and enhancing structural stability and performance under various dynamic loading conditions.

3 Numerical study

3.1 Benchmark building model

An 8-story benchmark isolated building, proposed by Yang et al. (1994), is utilized to implement the hybrid control system. The structure is equipped with a lead core rubber-bearing isolation

TABLE 4 Maximum base displacements and base floor displacement RMS under different control strategies and their reduction rate (RR).

Earthquakes	Control strategies and their respective reduction rate						
	BIS (m)	BIS + TMD (m)	RR (%)	BIS + ATMD (LQR) (m)	RR (%)	BIS + ATMD (ANN) (m)	RR (%)
Maximum base displacement							
Far Fault							
Chi-Chi	1.09	0.71	34.8	0.23	78.8	0.19	82.5
San Fernando	0.54	0.41	24	0.13	75.9	0.09	83.3
No Pulse Near Fault							
Kocaeli	1.01	0.65	35.6	0.22	78.2	0.13	87.1
Denali	0.68	0.52	23.5	0.21	69.1	0.13	80.8
Pulse Near Fault							
Landers	0.41	0.34	17	0.15	63.4	0.10	75.6
Kocaeli	0.52	0.39	25	0.10	80.7	0.09	82.6
Base floor displacement RMS							
Far Fault							
Chi-Chi	0.495	0.267	46	0.047	90.5	0.032	93.5
San Fernando	0.310	0.149	51.9	0.026	91.6	0.017	94.5
No Pulse Near Fault							
Kocaeli	0.478	0.320	33	0.068	85.7	0.039	91.8
Denali	0.372	0.187	49.7	0.035	90.5	0.027	92.7
Pulse Near Fault							
Landers	0.241	0.154	36.1	0.031	87.1	0.020	91.7
Kocaeli	0.296	0.216	27	0.039	86.8	0.024	91.8

system and an ATMD located on the base floor. The structural properties of each floor are summarized in Table 1.

3.2 ATMD tuning

An ATMD was coupled to the BIS to enhance its performance during seismic events and reduce structural vibrations, specifically the base isolation layer displacement. The tuning parameters for the passive part of the ATMD are determined using equations provided by Sadek et al. (1997) in terms of the non-dimensional parameters (Equation 24):

$$\mu = \frac{m_d}{M_T}, \gamma = \frac{1}{1 + \mu} \left[1 - \xi_s \sqrt{\frac{\mu}{1 + \mu}} \right], \xi_d = \xi_s \frac{1}{1 + \mu} + \sqrt{\frac{\mu}{1 + \mu}} \quad (24)$$

$$m_d = \mu M_T \quad (25)$$

$$c_d = 2\xi_d m_d \omega_d \quad (26)$$

$$k_d = \omega_d^2 m_d \quad (27)$$

where μ is the mass ratio between the ATMD mass, m_s , and the structure's total mass, M_T , $\gamma = \frac{\omega_d}{\omega_s}$ is the frequency ratio between the TMD and the structure's first frequency and ξ_d is the TMD damping ratio calculated with respect to the structure damping ratio $\xi_s = 5\%$. Being the total mass of the adopted base-isolated structure equal to $M_T = 3214.8$ tons, while its first natural frequency is $\omega_s = 2.2$ rad/s, having assumed a mass ratio $\mu = 0.05$, the TMD properties (Equations 25–27) are: $m_d = 160.74$ tons, $k_d = 694.59$ kN/m, and $c_d = 177.62$ kNs/m. It is worth noticing that the assumed mass ratio is in accordance with typical values adopted in literature for conventional TMD systems (Djedoui et al., 2016).

TABLE 5 Peak damper stroke for TMD, ATMD-LQR, and ATMD-ANN.

Earthquakes	TMD (m)	ATMD (LQR) (m)	ATMD (ANN) (m)
Far Fault			
Chi-Chi	0.711	0.239	0.194
San Fernando	0.410	0.134	0.094
No Pulse Near Fault			
Kocaeli	0.650	0.219	0.134
Denali	0.523	0.208	0.135
Pulse Near Fault			
Landers	0.337	0.149	0.104
Kocaeli	0.393	0.098	0.092

3.3 Base isolated system properties

The properties of the BIS are taken from Yang et al. (1994) and are detailed in Table 2.

3.4 LQR tuning

The inputs to the Artificial Neural Network (ANN) are derived from the structural response generated by a Linear Quadratic Regulator (LQR) controller, which requires the definition of the weighting matrices \mathbf{Q} and \mathbf{R} . These matrices play a crucial role in shaping the control performance by penalizing deviations in system states and excessive control effort, respectively. In this study, the system includes a single actuator associated with the ATMD. Consequently, the \mathbf{R} matrix is reduced to a scalar. A value of $R = 10^{-3}$ was selected to ensure a suitable trade-off between minimizing the control effort and achieving effective vibration mitigation.

The weighting matrix \mathbf{Q} is used to penalize deviations in selected state variables. Since the ATMD is directly connected to the BIS, the base displacement $x_b(t)$ and base velocity $\dot{x}_b(t)$ are key states to be regulated. To emphasize their importance in the control design, the diagonal elements corresponding to these variables, specifically $q_{1,1}$ and $q_{11,11}$, were set to 10^3 . This choice reflects the objective of reducing base motion without completely constraining it, consistent with the dynamic behavior expected in seismically isolated systems.

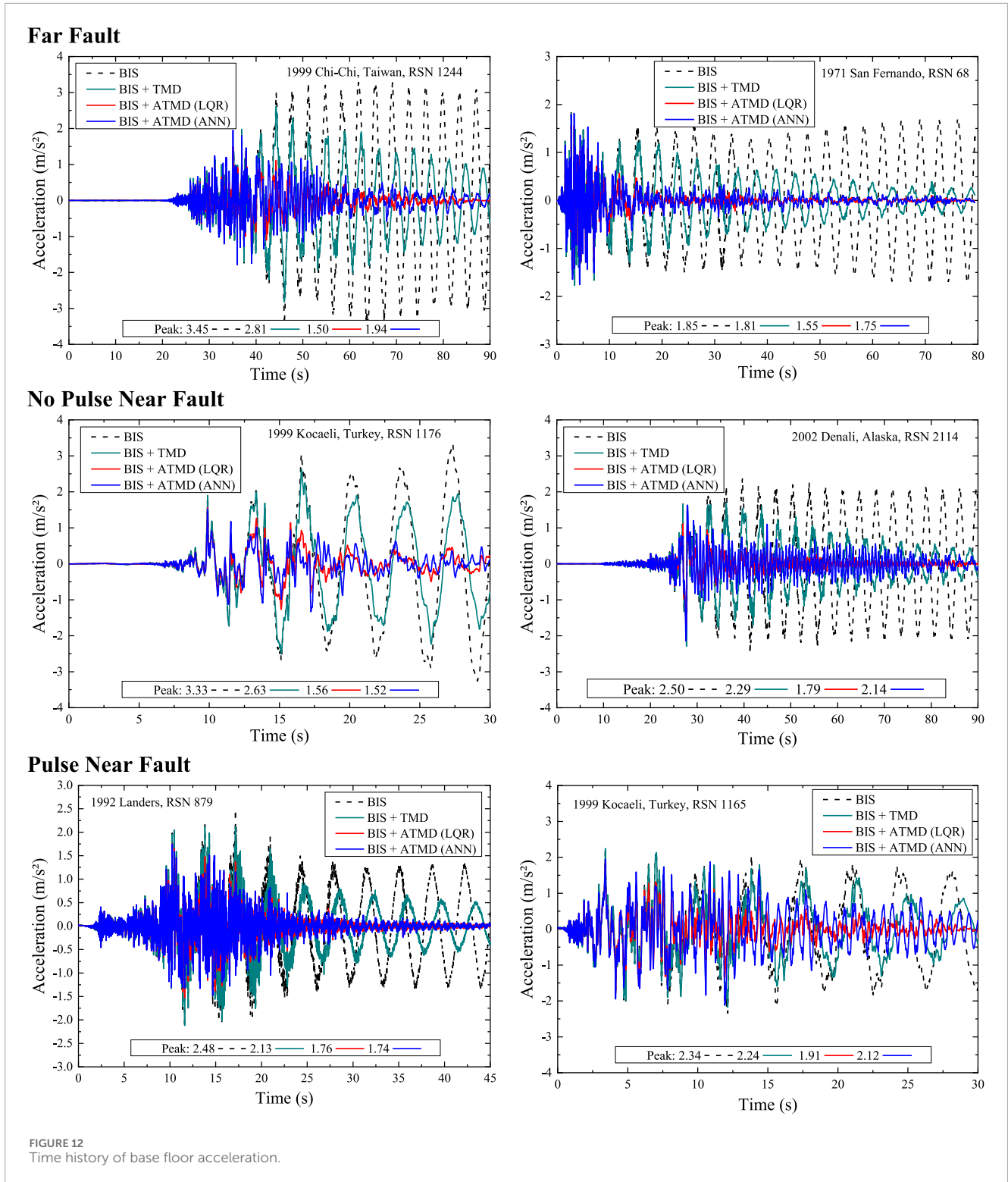
The values of \mathbf{Q} and \mathbf{R} were fine-tuned through an iterative trial-and-error process. Multiple numerical simulations were performed to assess the effectiveness of different combinations of weights. The configuration yielding the best compromise between vibration reduction and control effort was selected. The optimal control forces computed through the tuned LQR controller were then used as reference outputs for training the ANN model, enabling it to emulate the LQR behavior in real-time without relying on an explicit dynamic model during operation.

3.5 ANN tuning

The ANN-based controller is designed to regulate the ATMD system in real-time, with the objective of improving the seismic performance of an eight-story nonlinear base-isolated structure. The network is trained using data derived exclusively from a single natural earthquake record. Specifically, the ground motion from the 1940 El Centro earthquake was recorded at the Imperial Valley station, with a peak ground acceleration (PGA) of 0.32 g measured on the North/South component. The El Centro record was selected due to its broadband frequency content, which makes it a representative and widely adopted benchmark for training purposes. Once the optimal ANN model was identified through training, its generalization capability and robustness were evaluated by subjecting the structure to six additional earthquake records. These included both far-field and near-field events, with and without velocity pulses, to comprehensively assess the model's performance under a diverse range of seismic scenarios.

The process is illustrated in Figure 6, which outlines the step-by-step development and validation of the ANN-based controller. The procedure begins with programming a shear frame structure in MATLAB and applying an LQR controller, where the weighting matrices (\mathbf{Q} and \mathbf{R}) are optimized for improved performance. The ANN is then trained using the collected data, and the best-performing model is selected based on accuracy and error minimization. Finally, the trained ANN model is tested with six different earthquake records to evaluate its generalization and effectiveness. Training with historical earthquake data allows the ANN to learn, adjust, and reduce the differences between the LQR control force and the desired one, thereby enabling the ANN to approximate the optimal control strategy for which the LQR is known.

To assess the effectiveness of the ANN and ensure its emulation to the LQR, its structural response will be compared with that of the LQR controller itself, as well as with scenarios where no active control is applied.

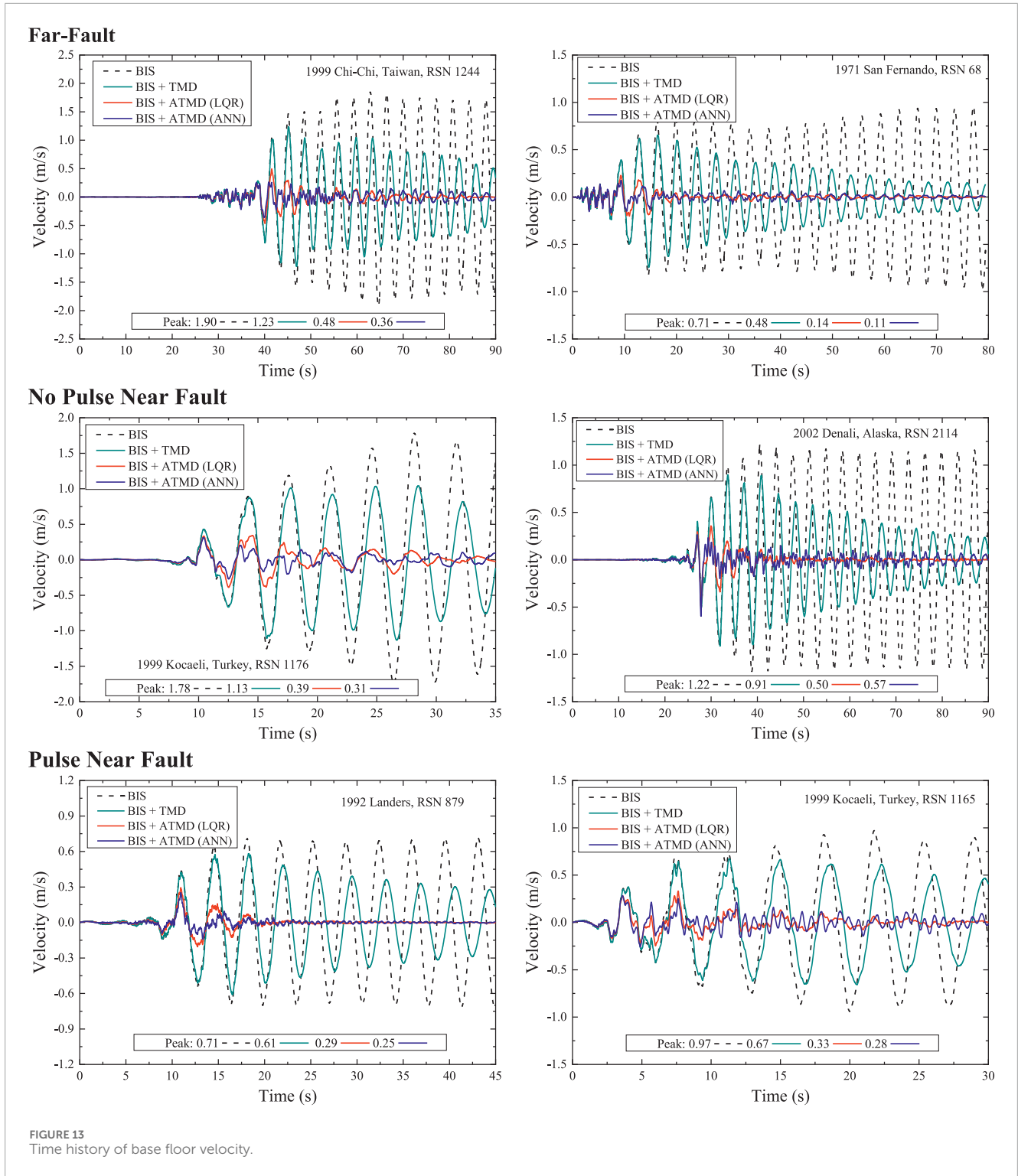


3.6 Earthquakes data set

The effectiveness of the ANN model within the hybrid system is evaluated by assessing it with six different real seismic recordings, each featuring diverse frequency components and peak accelerations. The seismic data for these six earthquakes, as sourced

from the Federal Emergency Management Agency (FEMA) P659 (Council, 2009), are presented in Table 3. To keep the structural behavior within a reasonable range, all the used records were scaled to a PGA of 0.2 g, as seen in Figure 7.

The utilized ground acceleration records are depicted in Figure 7.



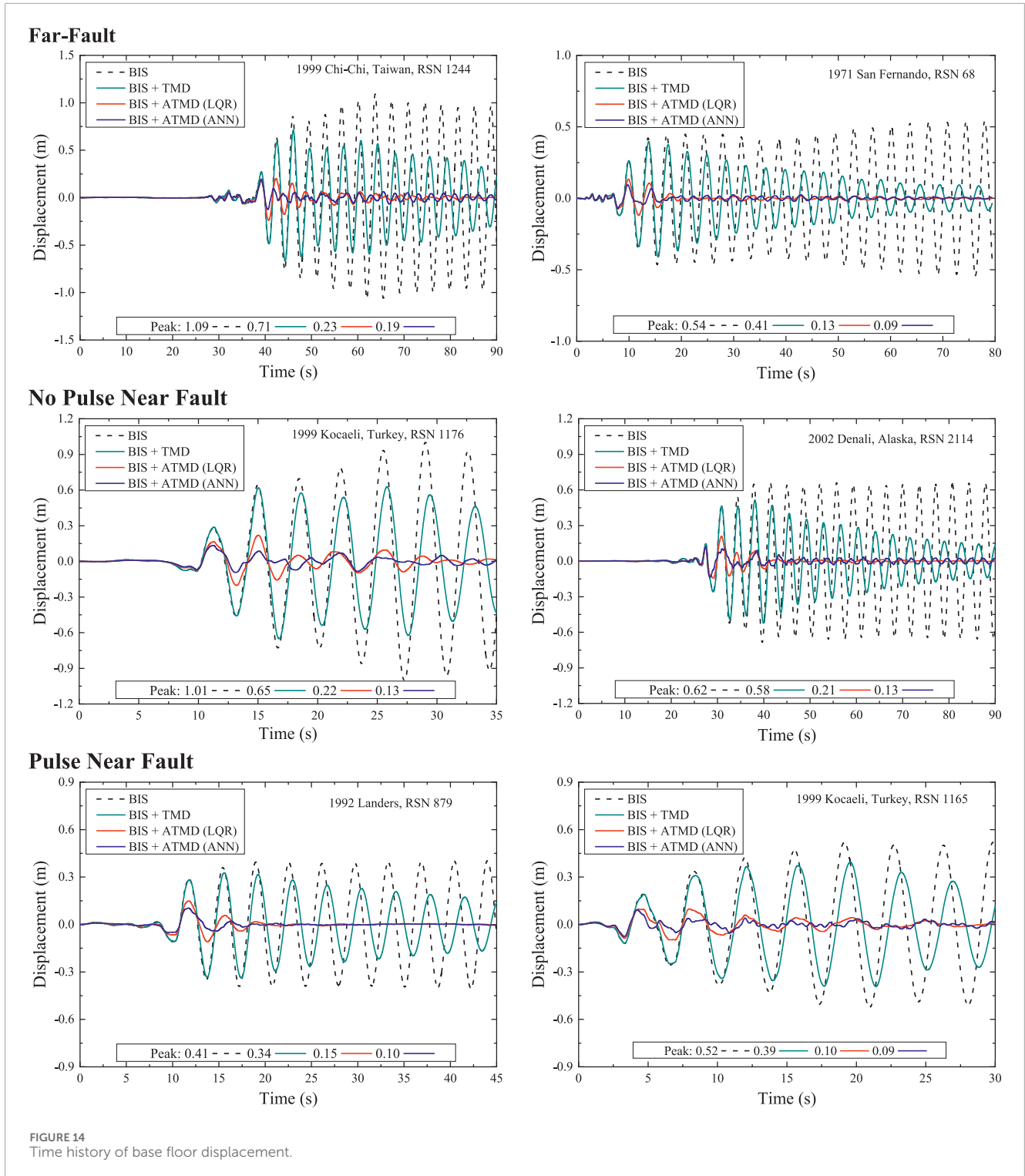
4 Results and discussion

4.1 ANN model training results

In this section, the evaluation of the ANN model's performance is made, employing the two key statistical metrics defined in Equations 22, 23 the *MSE* and the correlation coefficient *R*, are

evaluated. Furthermore, the model's predictive capability is assessed through the implementation of K-fold cross-validation.

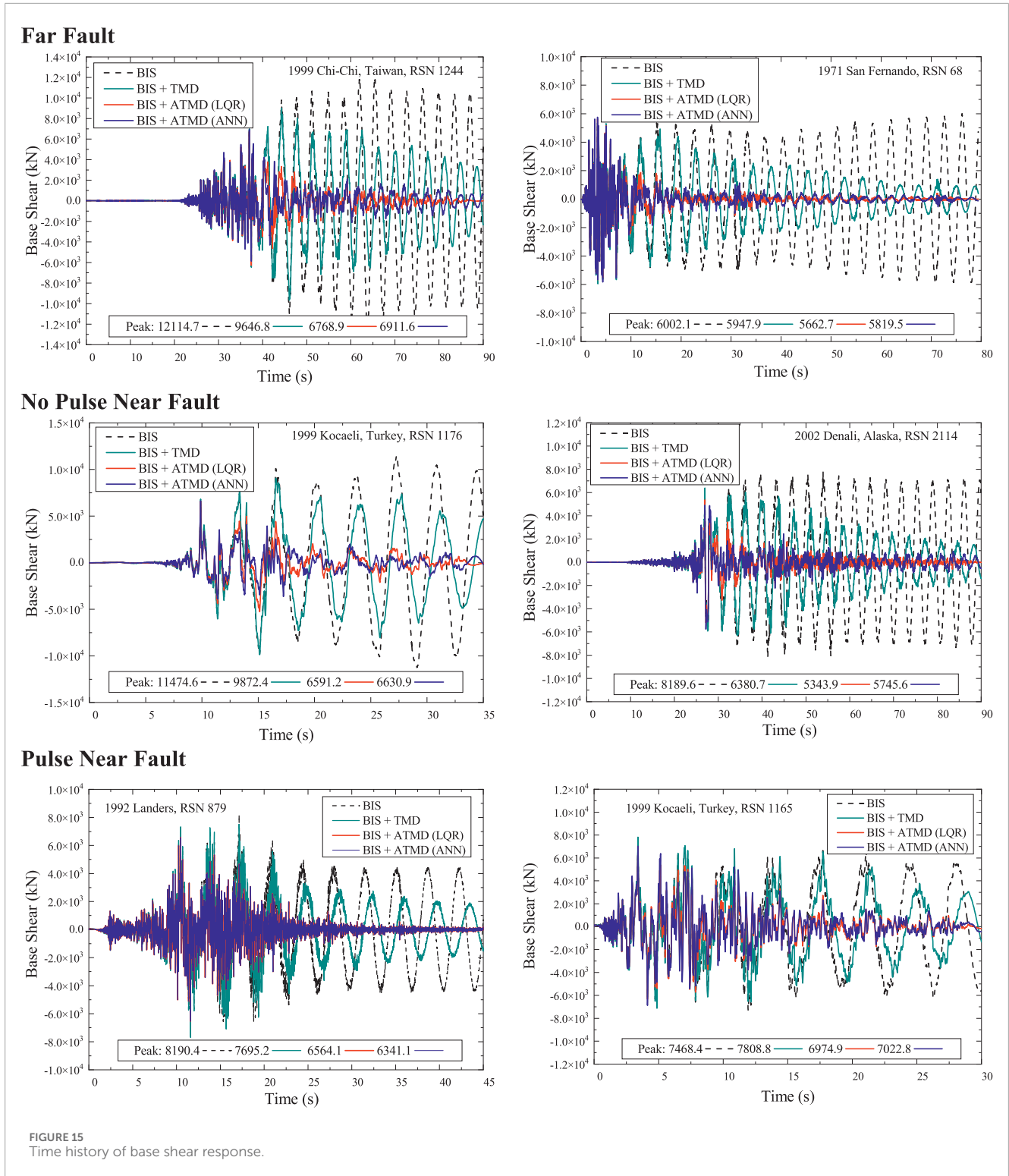
Figure 8 shows the *MSE* over 31 epochs, which highlights the model's accuracy and error dynamics. Initially, the *MSE* decreases sharply across training and validation datasets, indicating a reduction in prediction error as the model learns from the data. The close alignment of *MSE* values across datasets underscores the



model’s robustness. The best validation performance is observed at epoch 25, where the *MSE* reaches its minimum value of $3.3 \cdot 10^{-4}$. This epoch represents the point at which the model generalizes best to unseen data, striking an optimal balance between underfitting and overfitting, ensuring maximum predictive performance and minimal error between the output and the target. Beyond this point, *MSE* slightly increases, which may lead to overfitting.

Figure 9 shows the error histogram from the simulation of the optimal ANN model. The green bars indicate validation data, and the blue bars represent training data. Errors between the output and target values can be observed to lie within the range of -0.04 to 0.04 .

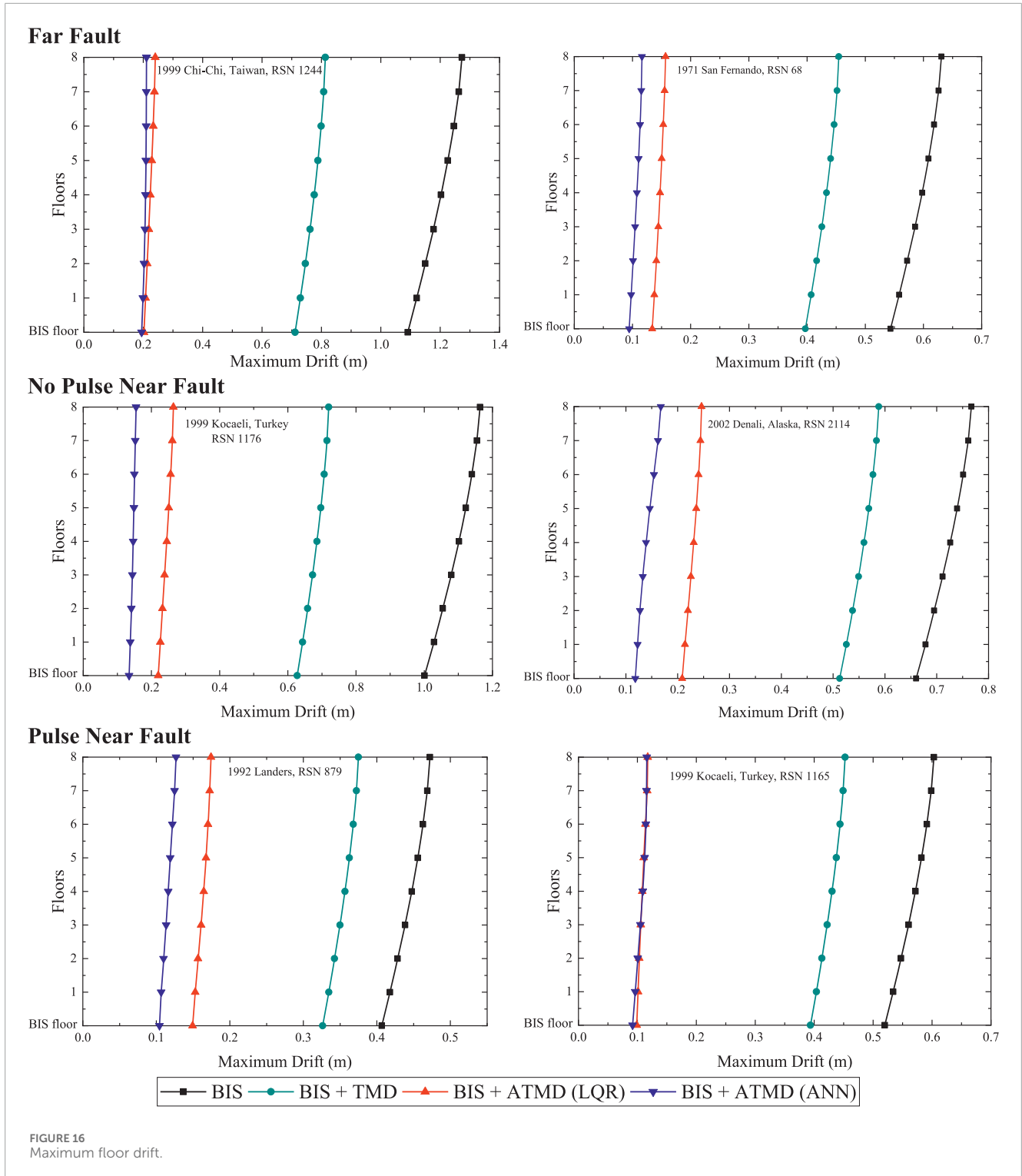
As defined in Equation 23, the correlation coefficient *R* measures the strength and direction of the linear relationship



between predicted and actual values, with higher values closer to 1 indicating stronger correlation and better predictive performance. Figure 10 displays scatter plots comparing the output and the target values of the control force in the optimal ANN model in the training phase, validation phase, and both phases. The results show strong correlation coefficients, with R values of 0.99115 for training and 0.99118 for

validation, which demonstrates the effective learning capability of the model.

The performance measures of the best ANN model are shown in Figure 11, revealing an R range of 0.98–0.99, where each column in the figure corresponds to a different fold in the K-fold cross-validation process, representing the model's performance across multiple training-validation splits.



This underscores the success of K-fold cross-validation in showcasing the model's robustness. The model consistently performs well across all five folds, effectively mitigating overfitting and underfitting risks, showcasing its remarkable ability to learn from training data and generate new data.

4.2 Performance assessment of ANN controller

After identifying the most effective neural network training model, it is utilized to control the ATMD through a feedback loop.

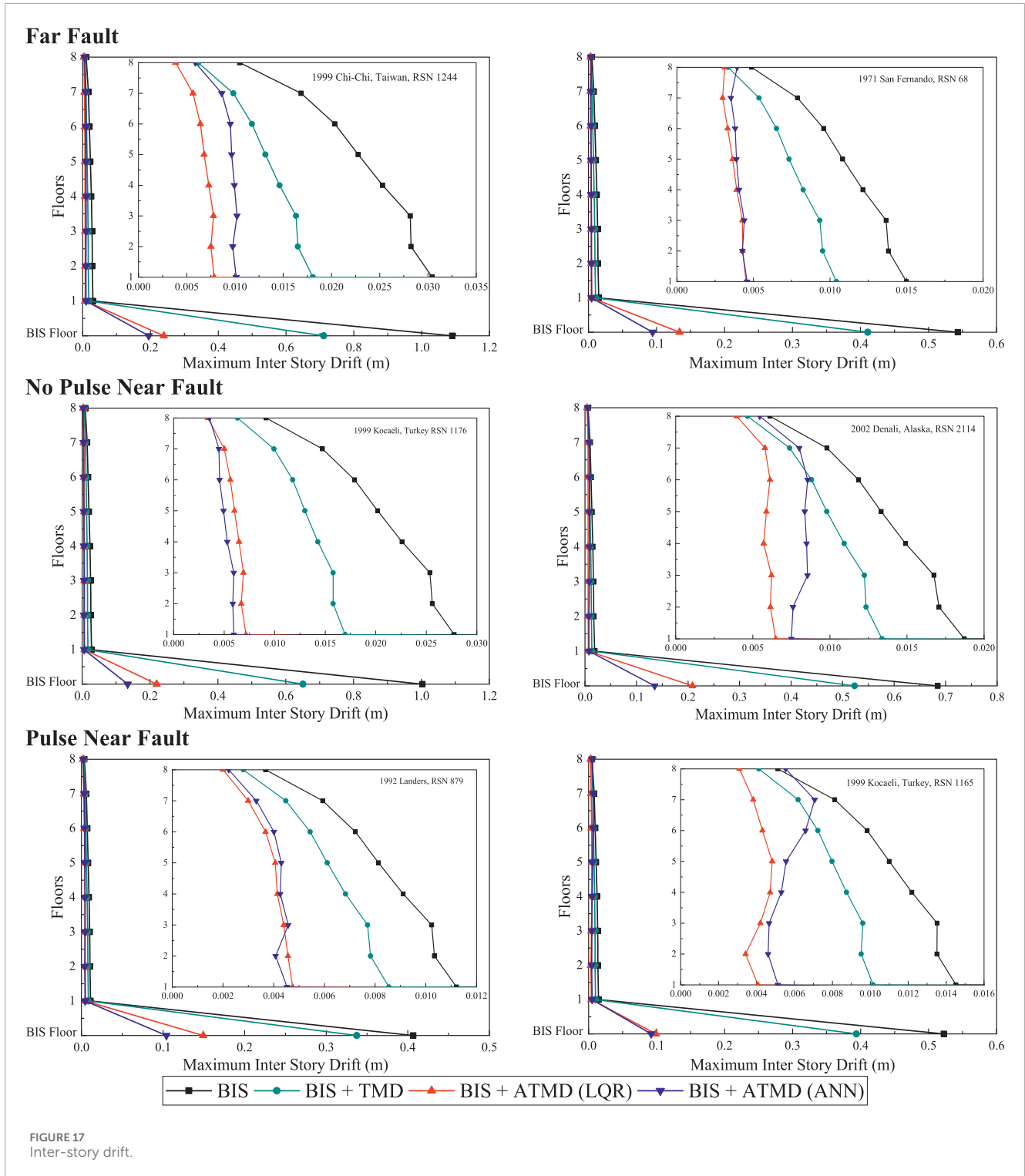


FIGURE 17 Inter-story drift.

This will enable computing the required control force to mitigate the effect of seismic activity on several ground motions to evaluate and validate the performance of the ANN model in adapting to new seismic conditions. For this purpose, the six ground motion records from the FEMA database not utilized during the training phase are selected (Table 3; Figure 7).

Various control strategies are considered to assess the performance of the ANN-driven ATMD. The control strategies adopted are:

- The base-isolated structure is equipped with a classical TMD, where the actuator force is set to null; this strategy is denoted BIS + TMD.

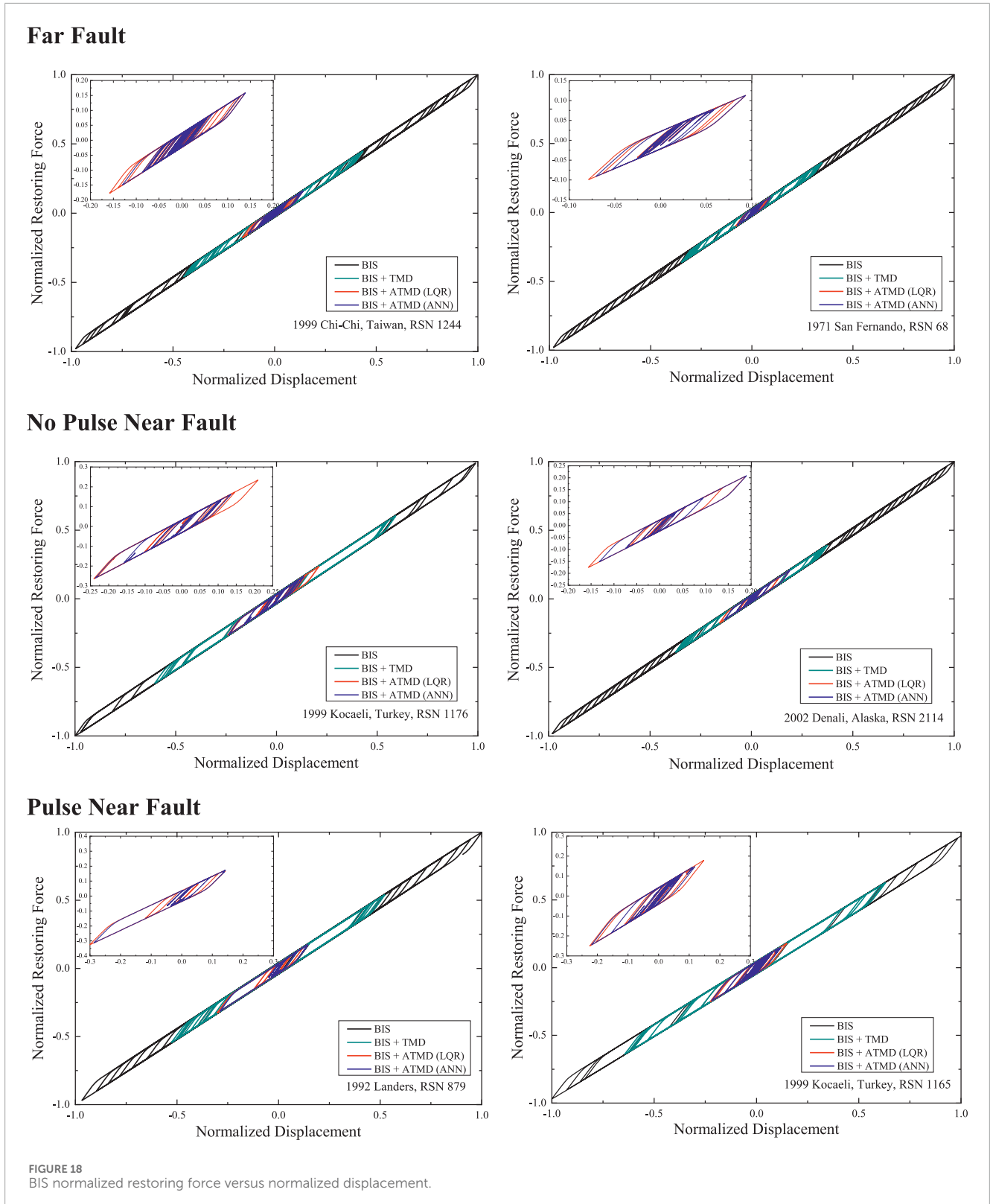


FIGURE 18 BIS normalized restoring force versus normalized displacement.

- The base-isolated structure is equipped with an ATMD driven by a LQR controller, denoted BIS + ATMD (LQR).
- The base-isolated structure is equipped with an ATMD driven by an ANN controller, denoted BIS + ATMD (ANN).

The first one has been compared with a hybrid control system employing only passive strategies. The performances of each control strategy are compared with those of BIS considered alone, and the results are reported in terms of reduction rate.

TABLE 6 Base floor displacement RMS values for the system controlled with ANN with and without delay.

Earthquakes	RMS delayed (m)	RMS non-delayed (m)
Far Fault		
Chi-Chi	0.035	0.032
San Fernando	0.021	0.017
No Pulse Near-Fault		
Kocaeli	0.042	0.039
Denali	0.033	0.027
Pulse Near-Fault		
Landers	0.024	0.020
Kocaeli	0.029	0.024

The dynamical parameters of interest investigated are the peak base floor displacement, the root mean square (RMS) of the base displacement, the peak control device stroke, the base floor acceleration, velocity and displacement time histories, the maximum drift and inter-story drift of all the floors and the hysteresis loops of the nonlinear isolator.

Table 4 presents the peak base displacement and the base displacement RMS for each control strategy under each earthquake, along with their respective reduction rate (RR) percentages evaluated across the six different earthquake scenarios. The passive TMD system provides moderate displacement reductions, ranging from 17% to 36%, showing its ability to mitigate vibrations to a certain extent. The active control strategy using LQR shows a more substantial improvement, reducing displacements by 63%–81%. Notably, the ANN-based ATMD demonstrates the highest effectiveness, consistently achieving displacement reductions between 81% and 87%, indicating its effectiveness and successful learning from the LQR controller. Further, the passive TMD system achieves moderate reductions in RMS values, ranging from 27% to 52%, indicating its limited yet consistent damping capacity. The ANN demonstrates reduction rates ranging from 91% to 94%, surpassing LQR's rates of 86%–92%. Similar to peak base displacement results, the ANN highlights its ability to learn from and surpass LQR's performance.

In addition to displacement and RMS evaluations, it is crucial to assess the stroke response of the damper systems to ensure their practical applicability. The stroke, defined as the peak displacement of the damper mass, determines the device's required motion range. Excessive stroke demands may render a control system impractical despite its effectiveness in reducing vibrations. Therefore, Table 5 presents a comparative analysis of the peak stroke displacements for the TMD, the LQR-controlled ATMD, and the ANN-controlled ATMD under the various earthquake records, offering insights into their mechanical feasibility alongside their control performance.

As shown in Table 5, the TMD system exhibits the highest stroke demands across all earthquake records, with peak values reaching

up to 0.711 m. In contrast, the LQR-controlled ATMD significantly reduces the required stroke, and the ANN-based ATMD achieves even lower stroke values in most cases. This demonstrates not only the superior control capability of the ATMD systems but also their mechanical efficiency. Notably, the ANN consistently maintains a lower stroke than LQR, confirming its intelligent control ability and practical feasibility.

Figure 12 illustrates for the six ground motions the base acceleration response of the nonlinear base-isolated structure comparing four scenarios: BIS, BIS and TMD, BIS and ATMD driven by the LQR controller, BIS and ATMD trained with the ANN controller. Applying TMD to the BIS is able to reduce the response better for far fault earthquakes than near fault ones. The graph reveals that the response can be further decreased by adopting the ATMD: a close performance between the ANN system and the LQR system in mitigating structural vibration for all the records is observed.

Figures 13, 14 illustrate the time history of base velocity and base displacement, respectively; it is evident that the ANN control system consistently achieves lower peak responses than the LQR control system; the adjustments of the control action in real time make this strategy more effective than applying only a TMD to limit base displacement and velocity. The response reductions occur across a wide range of earthquakes with different intensities and frequencies, which indicates that the ANN effectively adapts to the nonlinear behavior of the structure, providing better damping and stability.

The base shear force is shown in Figure 15 for the cases examined. The reduction observed with the hybrid control with ATMD helps to decrease seismic forces, thereby minimizing stress on structural components and reducing the risk of failure. Figure 15 illustrates how well active control methods are capable of minimizing the base shear across all seismic events and how this performance increases, especially for near fault earthquakes, compared to classical passive TMD. Notably, the ANN control exhibited nearly identical behavior to that of the LQR control, with only a slight increase observed in the maximum peak levels.

Figure 16 presents the maximum drift at all floors. The isolated structure exhibits significant drift for some earthquakes (Chi Chi, and Kocaeli earthquakes), indicating high susceptibility to seismic forces and potential structural damage. Applying a TMD to the base isolation layer can reduce the response to some extent; however, the LQR system shows markedly improved performance. ANN system performs even better, highlighting its superior efficiency in managing seismic responses. This reduced drift implies less structural damage and better protection.

The inter-story drift, depicted in Figure 17, shows that, again, both control methods based on ATMD effectively reduce the responses, especially at the lower floors, where the inter-story drift values are significantly minimized. While the LQR system shows superior performance, the ANN system also achieves notable reductions, closely miming the behavior of the LQR. This underscores the potential of ANN as a viable control strategy also compared to passive control with TMD.

Figure 18 illustrates the normalized restoring force of the BIS versus the normalized base displacement for the control strategies under six different testing earthquakes. Normalization is performed by dividing all the values by the maximum absolute value of the reference BIS responses, namely the restoring force and the base

TABLE 7 Base floor displacement RMS with and without noise.

Earthquakes	ATMD (LQR) (m)		ATMD (ANN) (m)	
	Without noise	With noise	Without noise	With noise
Far Fault				
Chi-Chi	0.047	0.051	0.032	0.033
San Fernando	0.026	0.029	0.017	0.017
Pulse Near-Fault				
Landers	0.031	0.036	0.020	0.026
Kocaeli	0.039	0.043	0.024	0.025
No Pulse Near-Fault				
Kocaeli	0.068	0.074	0.039	0.043
Denali	0.035	0.042	0.027	0.029

displacement. The addition of an ATMD to the BIS significantly reduces the energy dissipated by the isolator compared to the case where a classical TMD is added. This reduction is evident from the smaller peaks in the restoring force for both LQR and ANN controllers compared to the isolated structure. The decrease in the restoring force indicates lower hysteretic energy dissipation during seismic events, highlighting the ATMD's effectiveness in minimizing the relative motion between the building and its foundation.

Moreover, the ANN controller exhibits relatively smaller restoring force values, suggesting that it provides a more adaptive and efficient control strategy compared to the LQR controller. The ANN's ability to learn from data and predict optimal control actions allows it to handle the nonlinear behavior of the base isolation system more effectively.

4.3 Time delay effect on the response reduction

In order to emulate real-world conditions more accurately in the model, time delays were incorporated into the control loop of the model. Specifically, the structural responses sent to both LQR and ANN-based controllers were delayed by a one-time step. Additionally, the control forces generated by each controller were delayed by a one-time step before being applied via the actuator. This configuration resulted in an overall delay of two time steps within the control loop, effectively emulating the inherent delays present in practical applications.

The introduction of these delays revealed marked differences between the LQR and ANN approaches. When operating with a delayed full-state vector, the LQR encountered significant challenges in producing an effective control force. This difficulty highlighted concerns about the LQR's robustness and reliability in environments characterized by time delays, as the delayed response compromised its ability to maintain optimal control performance. The inherent limitations of the LQR in handling time delays emphasize the need

for alternative control strategies that can better cope with such conditions.

Conversely, the ANN demonstrated an excellent adaptability to time delays, consistently generating effective control forces and swiftly responding to mitigate structural responses. The ANN's performance remained robust despite the delays, showcasing its ability to adapt and learn from the delayed input data. This adaptability is attributed to the ANN's inherent capability to model complex, nonlinear relationships and its flexibility in handling dynamic changes within the system. The ANN's superior performance in the presence of time delays underscores its potential as a more reliable and effective control strategy in scenarios where delays are inevitable. These findings are confirmed in Table 6, which presents the root mean square (RMS) displacement results.

These findings underscore the potential advantages of employing ANN control strategies in scenarios where time delays are a critical factor. The adaptability and resilience of the ANN in the face of delays suggest that it can maintain high levels of control performance due to its natural ability to detect and react to nonlinearities, offering a significant improvement over traditional LQR methods. Therefore, incorporating ANN-based controllers in systems where time delays are prevalent could lead to more robust and efficient control solutions, ultimately enhancing the overall stability and performance of nonlinear systems.

4.4 Noise effect on the response reduction

Accurate measurement of dynamic response parameters such as base peak displacement, acceleration, velocity, inter-story drift, maximum drift, and base shear is critical for effective structural control. However, in real-world applications, sensor data is often contaminated with noise, which can compromise the accuracy and reliability of the measurements.

To address this challenge, this study investigates the impact of noise contamination on the performance of both the ANN

controller and the LQR controller. A white noise disturbance (Chen and Xu, 2008; Abdeddaim et al., 2017) is randomly generated and then integrated to obtain velocity and displacement signals. The obtained signals are summed with the displacement and velocity data during both the LQR simulation and the testing phase of the ANN to simulate noise contamination in sensors. The white noise peak acceleration is set to be 30 times less than the PGA of the earthquake.

The noise-affected responses were fed into both the LQR and ANN control systems within the feedback loop. Table 7 presents the base floor root mean square (RMS) under both LQR and ANN controllers with and without noise contamination for all the used records.

After introducing noise, a slight increase in the RMS displacement response was observed for both the LQR and ANN control methods. However, it was found that an effective solution to mitigate this increase is to adjust the control force. The robustness of the ANN controller was evaluated based on its ability to maintain control performance despite the presence of noise. Finally, this consistent effectiveness across different responses underscores ANN's potential to enhance structural resilience against seismic impacts.

5 Conclusion

This study aimed to enhance the seismic performance of nonlinear base-isolated structures by developing an AI-based hybrid control strategy that combines BIS with ATMDs, applying an ANN controller. The main objective was to design a control system capable of achieving effective seismic response mitigation with a limited number of sensors, thus improving practicality and cost-efficiency compared to conventional methods.

The methodology involved training an ANN controller using data generated from an LQR controller under seismic excitation with one ground motion data. The ANN model was trained to replicate the optimal control action of the LQR while addressing the nonlinear hysteretic behavior of the base-isolated structure. The controller's performance was validated through numerical simulations on an 8-story nonlinear base-isolated benchmark building subjected to various near-field and far-field earthquakes, including additional unseen earthquake records to assess generalization capabilities.

The major findings from the case study can be summarized as follows:

1. The ANN controller successfully captured the nonlinear behavior of the base isolators and structural responses, leading to more effective mitigation of seismic-induced vibrations compared to classical passive control (provided with classical TMD).
2. A reduction of over 80% in the base isolator displacement was achieved with the ATMD trained by the ANN, alongside a significant decrease in the RMS values of structural responses.
3. The ANN-based system demonstrated robustness against signal time delays and white noise contamination, ensuring reliable performance under realistic data conditions.
4. Effective control was achieved with only three sensors, highlighting a significant advantage over the conventional LQR controller, which requires full-state observation.

5. The ANN controller exhibited strong generalization capabilities, effectively mitigating structural responses during seismic events not included in the initial training dataset.
6. The ANN-driven control system provided real-time response capabilities, enabling immediate and adaptive adjustments to maintain structural integrity during earthquakes.

Moreover, the integration of BIS with ATMD further enhanced the energy dissipation capacity of the structure, leading to improved overall robustness against seismic events.

In conclusion, the proposed ANN-driven hybrid control approach demonstrated considerable potential for practical implementation by achieving comparable or superior performance to classical control methods while significantly reducing the complexity and cost associated with sensor deployment. Future research will focus on exploring more advanced ANN architectures, such as deep learning models, and conducting experimental validations on larger-scale structures to further assess the applicability of AI-based adaptive control in real-world scenarios. Additionally, the versatility of ANN-driven hybrid control strategies could be investigated in broader engineering contexts beyond seismic resilience.

Data availability statement

The raw data supporting the conclusions of this article will be made available by the authors, without undue reservation.

Author contributions

NG: Visualization, Formal Analysis, Data curation, Writing – original draft, Investigation, Software. MA: Writing – review and editing, Validation, Methodology, Supervision, Conceptualization. AO: Validation, Supervision, Writing – review and editing, Conceptualization. MB: Funding acquisition, Writing – review and editing, Supervision, Validation, Conceptualization, Investigation.

Funding

The author(s) declare that financial support was received for the research and/or publication of this article. This study has been supported by Universitas Mercatorum of Rome, Italy, under Grant No. 24-FIN/RIC (financial framework 2024).

Conflict of interest

The authors declare that the research was conducted in the absence of any commercial or financial relationships that could be construed as a potential conflict of interest.

Generative AI statement

The author(s) declare that no Generative AI was used in the creation of this manuscript.

Publisher's note

All claims expressed in this article are solely those of the authors and do not necessarily represent those of their affiliated

organizations, or those of the publisher, the editors and the reviewers. Any product that may be evaluated in this article, or claim that may be made by its manufacturer, is not guaranteed or endorsed by the publisher.

References

- Abdeddaim, M., Ounis, A., Shrimali, M. K., and Datta, T. K. (2017). Retrofitting of a weaker building by coupling it to an adjacent stronger building using MR dampers. *Struc Eng. Mech.* 62 (2), 197–208. doi:10.12989/sem.2017.62.2.197
- Aldwaik, M., and Adeli, H. (2014). Advances in optimization of highrise building structures. *Struct. Multidiscip. Optim.* 50, 899–919. doi:10.1007/s00158-014-1148-1
- Amezquita-Sanchez, J. P., Dominguez-Gonzalez, A., Sedaghati, R., de Jesus Romero-Troncoso, R., and Osornio-Rios, R. A. (2014). Vibration control on smart civil structures: a review. *Mech. Adv. Mater. Struct.* 21 (1), 23–38. doi:10.1080/15376494.2012.677103
- Banerjee, S., and Matsagar, V. (2023). Hybrid vibration control of hospital buildings against earthquake excitations using unbonded fiber-reinforced elastomeric isolator and tuned mass damper. *Buildings* 13 (7), 1724. doi:10.3390/buildings13071724
- Blachowski, B., and Pnevmatikos, N. (2018). Neural network based vibration control of seismically excited civil structures. *Period. Polytech. Civ. Eng.* 62 (3), 620–628. doi:10.3311/ppci.11601
- Brancati, R., Di Massa, G., Pagano, S., Petrillo, A., and Santini, S. (2020). A combined neural network and model predictive control approach for ball transfer unit–magnetorheological elastomer–based vibration isolation of lightweight structures. *J. Vib. Control* 26 (19–20), 1668–1682. doi:10.1177/1077546320902316
- Chang, J. C., and Soong, T. T. (1980). Structural control using active tuned mass dampers. *J. Eng. Mech. Div.* 106 (6), 1091–1098. doi:10.1061/jmcea3.0002652
- Chang, S., and Sung, D. (2019). Modal-energy-based neuro-controller for seismic response reduction of a nonlinear building structure. *Appl. Sci.* 9 (20), 4443. doi:10.3390/app9204443
- Charrouf, M. E., Ounis, A., Djedoui, N., and Abdeddaim, M. (2024). Analyzing seismic performance of optimized base isolation systems with soil–structure interaction: an analytical and numerical approach. *Pract. Periodical Struct. Des. Constr.* 29 (3), 04024032. doi:10.1061/ppscfx.sceng-1479
- Chen, B., and Xu, Y. L. (2008). Integrated vibration control and health monitoring of building structures using semi-active friction dampers: Part II—numerical investigation. *Eng. Struct.* 30 (3), 573–587. doi:10.1016/j.engstruct.2007.03.006
- Chen, P.-C., and Chien, K.-Y. (2020). Machine-learning based optimal seismic control of structure with active mass damper. *Appl. Sci.* 10 (15), 5342. doi:10.3390/app10155342
- Cheng, F. Y., and Jiang, H. (1998). Hybrid control of seismic structures with optimal placement of control devices. *J. Aerosp. Eng.* 11 (2), 52–58. doi:10.1061/(asce)0893-1321(1998)11:2(52)
- Conte, J. P., Durrani, A. J., and Shelton, R. O. (1994). Seismic response modeling of multi-story buildings using neural networks. *J. intelligent material Syst. Struct.* 5 (3), 392–402. doi:10.1177/1045589x9400500312
- Council, A. T. (2009). *Quantification of building seismic performance factors*. Redwood City, CA: US Department of Homeland Security, FEMA.
- Di Girolamo, G. D., Smarra, F., Gattulli, V., Potenza, F., Graziosi, F., and D'Innocenzo, A. (2020). Data-driven optimal predictive control of seismic induced vibrations in frame structures. *Struct. Control Health Monit.* 27 (4). doi:10.1002/stc.2514
- Djedoui, N., Ounis, A., and Abdeddaim, M. (2016). Active vibration control for base-isolated structures using a PID controller against earthquakes. *Int. J. Eng. Res. Afr.* 26, 99–110. doi:10.4028/www.scientific.net/jera.26.99
- Djedoui, N., Ounis, A., Pinelli, J., and Abdeddaim, M. (2017). Hybrid control systems for rigid buildings structures under strong earthquakes. *Asian J. Civ. Eng.* 18, 893–909.
- Djerouni, S., Ounis, A., Athamnia, B., Charrouf, M. E., Abdeddaim, M., and Djedoui, N. (2020). Optimal seismic response using a passive tuned mass damper inerter (TMDI). *J. Build. Mater. Struct.* 7 (1), 51–59. doi:10.34118/jbms.v7i1.208
- Elias, S., Beer, M., and Chen, J. (2025). Assessing seismic vulnerability of modular buildings under earthquake ground motions. *Eng. Struct.* 331, 120002. doi:10.1016/j.engstruct.2025.120002
- Elias, S., Djerouni, S., De Domenico, D., Abdeddaim, M., and El Ouni, M. H. (2023). Seismic response control of building structures under pulse-type ground motions by active vibration controller. *J. Low Freq. Noise, Vib. Act. Control* 42 (1), 345–367. doi:10.1177/14613484221130192
- Elias, S., and Matsagar, V. (2017). Research developments in vibration control of structures using passive tuned mass dampers. *Annu. Rev. Control* 44, 129–156. doi:10.1016/j.arcontrol.2017.09.015
- El Ouni, M. H., Abdeddaim, M., Elias, S., and Kahla, N. B. (2022). Review of vibration control strategies of high-rise buildings. *Sensors* 22 (21), 8581. doi:10.3390/s22218581
- Fisco, N. R., and Adeli, H. (2011a). Smart structures: Part I—active and semi-active control. *Sci. Iran.* 18 (3), 275–284. doi:10.1016/j.scient.2011.05.034
- Fisco, N. R., and Adeli, H. (2011b). Smart structures: Part II—hybrid control systems and control strategies. *Sci. Iran.* 18 (3), 285–295. doi:10.1016/j.scient.2011.05.035
- Ghanemi, N. E., Abdeddaim, M., and Ounis, A. (2024). Artificial intelligence-driven active tuned mass damper for enhanced seismic resilience of shear frame smart structures. *J. Vib. Eng. and Technol.* 12, 1577–1599. doi:10.1007/s42417-024-01491-0
- Ghanemi, N. E., Abdeddaim, M., and Ounis, A. (2023). “Seismic response reduction using an active tuned mass damper driven by an artificial neural network controller,” in *9th international conference on computational methods in structural dynamics and earthquake engineering methods in structural dynamics and earthquake Engineering*, 1227–1235.
- Gu, X., Yu, Y., Li, J., and Li, Y. (2017). Semi-active control of magnetorheological elastomer base isolation system utilising learning-based inverse model. *J. Sound Vib.* 406, 346–362. doi:10.1016/j.jsv.2017.06.023
- Hashemi, A., Jang, J., and Hosseini-Hashemi, S. (2022). Smart active vibration control system of a rotary structure using piezoelectric materials. *Sensors* 22 (15), 5691. doi:10.3390/s22155691
- Heertjes, M., and van de Wouw, N. (2006). Nonlinear dynamics and control of a pneumatic vibration isolator. *J. Vib. Acoust.* 128, 439–448. doi:10.1115/1.2128642
- Islam, B., Ahmed, N., Bhatti, D., and Khan, S. (2003). “Controller design using fuzzy logic for a twin rotor MIMO system,” *7th international multi topic conference, 2003 INMIC 2003* (IEEE).
- Ismail, M., Ikhouane, F., and Rodellar, J. (2009). The hysteresis Bouc-Wen model, a survey. *Archives Comput. methods Eng.* 16, 161–188. doi:10.1007/s11831-009-9031-8
- Jamil, M., Khan, M. N., Rind, S. J., Awais, Q., and Uzair, M. (2021). Neural network predictive control of vibrations in tall structure: an experimental controlled vision. *Comput. and Electr. Eng.* 89, 106940. doi:10.1016/j.compeleceng.2020.106940
- Jhang, S.-S., Lee, H.-J., Kim, C.-N., Song, C.-H., and Yu, W.-K. (2018). “ANN control for damping low-frequency oscillation using deep learning,” *Australasian universities power engineering conference (AUPEC)* (IEEE).
- Kalman, R. E. (1960). Contributions to the theory of optimal control. *Bol. Soc. Mat. Mex.* 5 (2), 102–119.
- Kim, H.-S. (2020). Development of seismic response simulation model for building structures with semi-active control devices using recurrent neural network. *Appl. Sci.* 10 (11), 3915. doi:10.3390/app10113915
- Kohavi, R. (1995). A study of cross-validation and bootstrap for accuracy estimation and model selection. *International joint conference on Artificial Intelligence (IJCAI)*. Montreal, QC.
- Lee, T.-Y., and Kawashima, K. (2007). Semiactive control of nonlinear isolated bridges with time delay. *J. Struct. Eng.* 133 (2), 235–241. doi:10.1061/(asce)0733-9445(2007)133:2(235)
- Li, C., Chang, K., Cao, L., and Huang, Y. (2021). Performance of a nonlinear hybrid base isolation system under the ground motions. *Soil Dyn. Earthq. Eng.* 143, 106589. doi:10.1016/j.soildyn.2021.106589
- Linderman, L. E., and Spencer, Jr B. (2016). Decentralized active control of multistory civil structure with wireless smart sensor nodes. *J. Eng. Mech.* 142 (10), 04016078. doi:10.1061/(asce)em.1943-7889.0001126
- Liut, D., Mathieu, E., Singh, M., and Mook, D. (1999). Neural-network control of building structures by a force-matching training scheme. *Earthq. Eng. Struct. Dyn.* 28 (12), 1601–1620. doi:10.1002/(sici)1096-9845(199912)28:12<1601::aid-eeq884>3.0.co;2-g
- Lu, P., Chen, S., and Zheng, Y. (2012). Artificial intelligence in civil engineering. *Math. Problems Eng.* 2012, 1–22. doi:10.1155/2012/145974
- Mardani, A., Jusoh, A., and Zavadskas, E. K. (2015). Fuzzy multiple criteria decision-making techniques and applications—Two decades review from 1994 to 2014. *Expert Syst. Appl.* 42 (8), 4126–4148. doi:10.1016/j.eswa.2015.01.003
- Mazza, F., Donnici, A., and Labernarda, R. (2023). Seismic vulnerability of fixed-base and base-isolated hospitals: blind comparison between shaking table and numerical tests. *Procedia Struct. Integr.* 44, 147–154. doi:10.1016/j.prostr.2023.01.020

- Mazza, F., Donnici, A., and Labernarda, R. (2024). Structural and non-structural numerical blind prediction of shaking table experimental tests on fixed-base and base-isolated hospitals. *Earthq. Eng. Struct. Dyn.* 53 (10), 2961–2987. doi:10.1002/eqe.4146
- Mazza, F., and Labernarda, R. (2022). Effects of near-fault acceleration and non-acceleration pulses on pounding between in-plan irregular fixed-base and base-isolated buildings. *Struct. Control Health Monit.* 29 (9), e2992. doi:10.1002/stc.2992
- Moghaddasie, B., and Jalaeifar, A. (2019). Optimization of LQR method for the active control of seismically excited structures. *Smart Struct. Syst.* 23 (3), 243–261. doi:10.12989/sss.2019.23.3.243
- Naeim, F., and Kelly, J. M. (1999). *Design of seismic isolated structures: from theory to practice*. John Wiley and Sons.
- Neves, A. C., Gonzalez, I., Leander, J., and Karoumi, R. (2017). Structural health monitoring of bridges: a model-free ANN-based approach to damage detection. *J. Civ. Struct. Health Monit.* 7, 689–702. doi:10.1007/s13349-017-0252-5
- Pandey, S. K., and Laxmi, V. (2015). “Optimal control of twin rotor MIMO system using LQR technique,” in *Computational intelligence in data mining-volume 1* (New Delhi: Springer), 11–21.
- Phillips, A., and Sahin, F. (2014). “Optimal control of a twin rotor MIMO system using LQR with integral action,” *2014 world automation congress (WAC)* (IEEE).
- Radmard Rahmani, H., Chase, G., Wiering, M., and Könke, C. (2019). A framework for brain learning-based control of smart structures. *Adv. Eng. Inf.* 42, 100986. doi:10.1016/j.aei.2019.100986
- Reynaldi, A., Lukas, S., and Margaretha, H. (2012). *Backpropagation and levenberg-marquardt algorithm for training finite element neural network. 2012 sixth UKSim/AMSS European symposium on computer modeling and simulation* (IEEE).
- Sabetahd, R., Mousavi Ghasemi, S. A., Vafaei Poursorkhabi, R., Mohammadzadeh, A., and Zandi, Y. (2022). Response attenuation of a structure equipped with ATMD under seismic excitations using methods of online simple adaptive controller and online adaptive type-2 neural-fuzzy controller. *Comput. Intell. Neurosci.* 2022, 1–25. doi:10.1155/2022/5832043
- Sadek, F., Mohraz, B., Taylor, A. W., and Chung, R. M. (1997). A method of estimating the parameters of tuned mass dampers for seismic applications. *Earthq. Eng. Struct. Dyn.* 26 (6), 617–635. doi:10.1002/(sici)1096-9845(199706)26:6<617::aid-eeq664>3.0.co;2-z
- Sanad, A., and Saka, M. (2001). Prediction of ultimate shear strength of reinforced-concrete deep beams using neural networks. *J. Struct. Eng.* 127 (7), 818–828. doi:10.1061/(asce)0733-9445(2001)127:7(818)
- Sapountzakis, E., Florakis, G., and Kapasakalis, K. (2024). Design and performance assessment of base isolated structures supplemented with vibration control systems. *Buildings* 14 (4), 955. doi:10.3390/buildings14040955
- Shin, J.-H., Kwak, M. K., Kim, S.-M., and Baek, K.-H. (2020). Vibration control of multi-story building structure by hybrid control using tuned liquid damper and active mass damper. *J. Mech. Sci. Technol.* 34 (12), 5005–5015. doi:10.1007/s12206-020-1105-4
- Sibi, P., Jones, S. A., and Siddarth, P. (2013). Analysis of different activation functions using back propagation neural networks. *J. Theor. Appl. Inf. Technol.* 47 (3), 1264–1268.
- Skinner, R. I., Robinson, W. H., and McVerry, G. H. (1993). An introduction to seismic isolation.
- Smarra, F., Girolamo, G. D. D., Gattulli, V., Graziosi, F., and D’Innocenzo, A. (2020). Learning models for seismic-induced vibrations optimal control in structures via random forests. *J. Optim. Theory Appl.* 187 (3), 855–874. doi:10.1007/s10957-020-01698-7
- Smith, G. N. (1986). “Probability and statistics in civil engineering,” in *Collins professional and technical books*, 244.
- Subasri, R., Natarajan, A., Sundaram, S., and Jianliang, W. (2013). *Neural aided discrete PID active controller for non-linear hysteretic base-isolation building. 2013 9th Asian Control Conference ASCC* (IEEE).
- Ulusoy, S., Bekdaş, G., Nigdeli, S. M., Kim, S., and Geem, Z. W. (2021). Performance of optimum tuned PID controller with different feedback strategies on active-controlled structures. *Appl. Sci.* 11 (4), 1682. doi:10.3390/app11041682
- Ümütlü, R. C., Ozturk, H., and Bidikli, B. (2021). A robust adaptive control design for active tuned mass damper systems of multistory buildings. *J. Vib. Control* 27 (23–24), 2765–2777. doi:10.1177/1077546320966236
- Wen, Y. (1989). Methods of random vibration for inelastic structures. *Appl. Mech. Rev.* 42, 39–52. doi:10.1115/1.3152420
- Wen, Y.-K. (1976). Method for random vibration of hysteretic systems. *J. Eng. Mech. Div.* 102 (2), 249–263. doi:10.1061/jmcea3.0002106
- Yang, J., Li, Z., Danielians, A., and Liu, S. (1992). Aseismic hybrid control of nonlinear and hysteretic structures I. *J. Eng. Mech.* 118 (7), 1423–1440. doi:10.1061/(asce)0733-9399(1992)118:7(1423)
- Yang, J., Li, Z., and Vongchavalitkul, S. (1994). Generalization of optimal control theory: linear and nonlinear control. *J. Eng. Mech.* 120 (2), 266–283. doi:10.1061/(asce)0733-9399(1994)120:2(266)
- Yang, S.-M., Chen, C.-J., and Huang, W. (2006). Structural vibration suppression by a neural-network controller with a mass-damper actuator. *J. Vib. Control* 12 (5), 495–508. doi:10.1177/1077546306064269
- Ying, W., Chong, W., Hui, L., and Renda, Z. (2009). “Artificial neural network prediction for seismic response of bridge structure,” in *2009 international conference on artificial intelligence and computational Intelligence*, 503–506.
- Zahedin Labaf, D., De Angelis, M., and Basili, M. (2023). Multi-objective optimal design and seismic assessment of an inerter-based hybrid control system for storage tanks. *Bull. Earthq. Eng.* 21 (3), 1481–1507. doi:10.1007/s10518-022-01457-1
- Zhang, J., and Xue, Y. (2023). Intelligent control method research for high rise building vibration by integrating genetic algorithm and LSTM. *IEEE Access* 12, 9810–9821. doi:10.1109/access.2023.3348145